Supporting online material

Materials and Methods

Tissue Collection

Tissues were procured from cases admitted during the period 2005-2007 to the Department of Forensic Medicine, Karolinska Institute, after receiving consent from relatives. Some heart samples were obtained from the UK Human Tissue Bank, Great Britain. Ethical permission for this study was granted by the Karolinska Institutet Ethical Committee. Human left ventricular tissue without the septum was dissected. Hearts were dissected and clotted blood was removed from the chambers before the heart weights were determined in accordance with the European Recommendation on the harmonization of medico-legal autopsy rules (*1, 2*). Then, epicardial fat and visible blood vessels were removed and the tissues were stored at –80 °C until analysis.

Nuclear Isolation

Left ventricular tissue (apex and wall) was thawed and whole-thickness samples were trimmed using a scalpel. Approximately 10g of tissue was added to 200mL of ice cold lysis buffer (0.32 M sucrose, 5 mM $CaCl_2$, 3mM magnesium acetate, 2.0 mM EDTA, 0.5 mM EGTA, 10 mM Tris-HCl (pH 8.0), 1 mM DDT) with a proteinase inhibitor cocktail (Sigma). All subsequent steps were performed on ice. The mixture was blended (Braun 600W blender) at speed turbo 9 for 10 minutes. The crude suspension was further homogenized by an Ultra-Turrax® homogenizer (IKA) at 20,000 rpm for 8 seconds. Triton X-100 was added to a final concentration of 0.2%, before the suspension was

dounced with a type A pestle exactly eight strokes in a glass douncer. The solution was put through a large filter sieve twice. Then, two layers of cotton gauze were placed on top of the sieve, and the solution was filtered two more times. This solution was consecutively filtered in 100 and 70 micron filters (Falcon) and equally divided into six 50 ml tubes. These tubes were centrifuged for 8 minutes at 1000g at 4 °C. The supernatant was carefully removed with a pipette from each tube and then discarded. The crude nuclear pellets were resuspended with 30 ml of 2.1 M sucrose solution (2.1 M sucrose, 3 mM magnesium acetate, 1 mM DTT, 10 mM Tris-HCl, pH 8.0). This was then layered onto a cushion of 10 ml 2.2 M sucrose solution (2.2 M sucrose, 3 mM magnesium acetate, 1 mM DTT, 10 mM Tris-HCl, pH 8.0), and centrifuged at 30,000g for one hour at 4°C. The supernatant was carefully pipetted off and discarded. The side of the tube was also carefully wiped to avoid supernatant contamination to the pellet. The pellet from each tube was then resuspended with 1,5 ml of nuclei buffer (0.43 M sucrose, 70 mM KCl, 2 mM MgCl2, 10 mM Tris-HCl (pH 7.2), 5 mM EGTA).

For the mixed heart/brain experiment, both tissue from the occipital cortex and left ventricle where processed together. Apart from an adjusted sucrose concentration of 2.0M, all procedures were performed as described above.

Flow Cytometry

Cardiomyocyte nuclei were isolated and collected using flow cytometry. A mouse monoclonal antibody to cTroponin I (Chemicon™, Millipore, MAB 3152), a polyclonal rabbit antibody to cTroponin T (Abcam, ab10224), or isotype control antibodies were directly conjugated to Alexa Fluor® 488 or 647 (Alexa Fluor® 488 or 647 Monoclonal

Antibody Labeling Kits, Molecular Probes™, Invitrogen). Antibodies to cTroponin T and cTroponin I were used at 1:800 to label cardiomyocyte nuclei, and left to incubate on ice for at least 30 minutes. Single nuclei (independent of their DNA content) were separated from doublets or higher-order aggregates by using a gating strategy using only physical parameters (*3*). Briefly, singlets were defined as a function of forward scatter width (FSC-W) and forward scatter height (FSC-H) which was defined based on the fluorescent intensity of the DNA stain DRAQ5®. All single nuclei, independent of their DNA content were detected within the defined gate (*4*), making it easy to discriminate singlets from doublets and other nuclei aggregates. All flowcytometric nuclei sorts were performed using the described sorting strategy.

For flow cytometry sorts of diploid and polyploidy cardiomyocyte nuclei and analysis of cardiomyocyte nuclei ploidy levels, nuclei were labeled with cTroponinT/I antibodies as described and DNA content was visualized with Hoechst33342 dye (5ug/ml) (Invitrogen, Molecular Probes®). Hoechst 33342 (5ug/ml) did not influence ^{14}C levels in cardiomyocyte DNA (n=5; p=0.69, Mann-Whitney test).

Purity of flowcytometrically sorted nuclei was confirmed by reanalyzing the sorted populations. ^{14}C levels were corrected if sorting purity was less than 100% (see Flow cytometry purity). For the mixed brain/heart experiment, we used the labeling protocol as described before (*3*). Brain tissue (occipital cortex) was homogenized together with left ventricular heart tissue. Nuclei were isolated as described before, incubated for 1-5h hours at 4°C and subsequently labeled with NeuN (Millipore, mab 377), cTroponinT and cTroponinI antibodies directly conjugated to Alexa® 488/647 dyes. All flowcytometric

experiments were performed by using a FACSVantage DiVa instrument (BD Bioscience).

Immunocytochemistry

Nuclear isolates were incubated for 30 min with an antibody to cTroponin T (1:800, Abcam, ab10224) or cTroponin I (1:800, Chemicon™, Millipore, MAB 3152) directly conjugated to Alexa Fluor® 488. Nuclei were counterstained with DAPI and transferred to slides. Pictures were taken with a Zeiss Meta® confocal microscope (Zeiss) and edited with Photoshop (Adobe®) software.

Gene expression of sorted nuclei.

Nuclei isolates were labeled with a cTroponin T antibody (Abcam, ab10224) and flow cytometric sorted according to their immunoreactivity. Total RNA was extracted from cTroponin T positive and negative populations (5-10 million nuclei), respectively, using the RNeasy mini plus kit (Qiagen). Equal amounts of total RNA from each sample was reverse transcribed to cDNA using the QuantiTect RT kit (Qiagen). In a final volume of 50 μL, 7.5 ng of cDNA was amplified with POWER SYBR PCR® master mix (Applied Biosystems) and primers (Eurofins MWG Operon). The primer pairs for cTroponin T (TNNT2), cTroponin I (TNNI3), Nkx2.5, vWF, vimentin, smooth muscle actin (ACTA2), CD45 and 28S ribosomal RNA (28S rRNA) were designed by using Primer3-BLAST ((*5*),NCBI, USA) and selected to yield a single amplicon based on dissociation curves. Quantitative real-time PCR was performed with a PRISM 7300 (Applied Biosystems). The relative mRNA levels were calculated using the C_t method, using 28S rRNA as a

normalizer. cTroponin T-positive nuclei served as a reference for TNNT2, TNNI3 and Nkx2.5. cTroponin T negative sorted nuclei served as a reference for vWF, vimentin, ACTA2 and CD45.

Western blot

Flow cytometry isolated nuclei ($1x10^6$) were spun down at $1.2x10^3$ g at 4°C for 15 minutes and lysed in RIPA lysis buffer (50 mM Tris, pH 7.2, 150 mM NaCl, 2 mM EDTA, 1% NP-40, 1% sodium deoxycholate, and 0.1% v/v SDS) supplemented with protease inhibitor cocktail (Roche) and separated by 10% or 12% SDS-PAGE. Equivalent amounts of whole human heart and brain tissues, or the heart cytoplasmic and nuclear fractions, were lysed in RIPA buffer. The proteins were transferred onto nitrocellulose membranes (Schleicher & Schuell) which were blocked in 5% milk and incubated at 4°C overnight with the following antibodies: cTroponin I (1:1000, mouse, Chemicon™, Millipore, MAB3152), cTroponin T (1:1000, rabbit, Abcam ab10224), cTroponin T 1:1000 (mouse, Abcam ab10214), Nkx 2.5 (1:500, mouse, R&D, MA2444), GATA4 (1:500, goat, R&D, AF2606), ERK1/2 (p44/p42 MAP kinase, 1:500, rabbit, Cell Signaling, 9102), αPAK (1:1000, rabbit, Santa Cruz (C-19)), TOM20 (1:5000, rabbit, Santa Cruz (FL-145)) or Histone3 (1:10 000, rabbit, Abcam, ab1791). Membranes were then incubated with the appropriate HRP-conjugated secondary antibody (1:2000; Amersham Biosciences,and Abcam) in 5% milk and detection was performed using ECL reagent and Hyperfilm (both from Amersham Biosciences).

Extraction of DNA

DNA extraction was performed as previously described (*6*). Briefly, isolated nuclei were suspended in 1 ml of 1% SDS, 5 mM EDTA-Na_2, 10 mM Tris-HCl, pH 8.0) and 8 µl of protease K solution (20 mg/ml, Invitrogen). The sample tube was then gently inverted numerous times and then incubated at 65°C overnight, with intermittent tube inversions. RNAse cocktail (8 µl, Ambion) was then added to each sample. Further 60 min incubation with inversions was then done. Three ml of a solution of sodium iodide (7.6 M NaI, 20 mM EDTA-Na_2, 40 mM Tris-HCl, pH 8.0) was then mixed to each sample followed by repeated inversion. Afterwards, 6 ml of filtered 99% ethanol was added and tubes gently inverted numerous times until the DNA precipitated. The DNA pellet was then washed in baths of 70% ethanol for 15 minutes for three times. Lastly, the DNA was rinsed in a water bath for 5 seconds, and then carefully transferred to a glass storage tube. The DNA pellet was resuspended in water after being thoroughly dried and then left to incubate up to seven days at 65°C, with many inversions, in order to completely dissolve the DNA into the water. The amount of DNA was quantified using spectrophotometry and only samples within a defined range (260/280: 1.8-2.0; 260/230: 2.0-2.4) were included into data analysis. In order to determine precisely remaining protein impurities all samples were additionally analyzed by means of HPLC. The mean protein contamination was 0.84%±0.17 SEM. Moreover, contamination by unidentified carbon sources can be detected by comparing the expected carbon content from the analyzed amount of DNA and the actual carbon content in the sample, which is measured in the accelerator mass spectrometry analysis. If a sample would contain more carbon than can

be accounted for by the DNA, this would mean that it was contaminated, but this was never the case.

Accelerator mass spectrometry

Accelerator mass spectrometry (AMS) analysis was performed blind to the identity of the sample. The DNA in water was moved to quartz AMS combustion tubes. They were then evaporated in a lyophilizer. Once completely dry, excess copper oxide (CuO) was introduced to each sample, the air was evacuated completely, and then sealed off with a H_2/O_2 torch. In order to completely combust all carbon to CO_2, these samples were then put into a 900°C furnace for 3.5 hours. The CO_2 that evolved during this process was then purified, trapped, and subsequently reduced to graphite in the presence of an iron catalyst in individual reactors (*7, 8*). CO_2 samples greater than 500 μg were split and the $\delta^{13}C$ measurement was attained by stable isotope ratio mass spectrometry. The graphite targets were then measured blindly at the Center for Accelerator Mass Spectrometry at Lawrence-Livermore National Laboratory, California, USA. A $\delta^{13}C$ correction of –23 +/- 2 was used for all samples (*9*). Background contamination corrections during the process of each AMS sample preparation were done according to the procedures of Brown and Southon (*10*). Each sample's measurement of error had values that ranged between ±2-10‰ (1 SD) $\Delta^{14}C$. Following the usual convention (*9*), all of the ^{14}C data are reported as decay corrected $\Delta^{14}C$ values since it is the most widespread for reporting post-bomb radiocarbon data (*9, 11*).

Bioinformatics

The following RefSeq sequences of human cTroponin T (TNNT2) and human cTroponin I (TNNI3) from NCBI were analyzed computationally for subcellular location. TNNT2: H. sapiens (NP_000355), M. musculus (AAH63753.1), G. gallus (NP_990780.1), closest D. melanogaster homologue by BLAST is upheld (NP_001014738.1; isoform F displayed highest number of NLS), C. elegans (NP_001024704.1). TNNI3: H. sapiens (NP_000354), M. musculus (NP_033432.1), G. gallus (NP_998735.1), D. melangogaster closest homologues wings up (NP_728141.1) and C. elegans (NP_507250.1).

Flow cytometry purity

In the case where sample purity of the cTroponin I-positive or cTroponin T-positive population was less than 100%, we corrected the measured ^{14}C levels applying the following equations. (*a*: purity of the cTroponin-positive population in %; *b*: measured ^{14}C value for the cTroponin-positve population; *c*: measured ^{14}C value for the unsorted population; *d*: ratio of cTroponin-positive nuclei in % (DNA weighted); *x*: purity corrected ^{14}C value for the cTroponin-positive population; *y*: purity corrected ^{14}C value for the cTroponin-negative population)

I $b*100 = x*a + y*(100-a)$ ***II*** $c*100 = x*d + y*(100-d)$

The equations were then solved for *x*.

III $x = (-100*c + c*a + 100*b – b*d)/(a-d)$

^{14}C value correction for polyploidisation

Nuclei isolates were incubated in Hoechst 33342 (5ug/ml) and DNA content was determined by flow cytometry (fig. S5A). The average DNA content per cardiomyocyte nuclei was calculated by establishing the arithmetic mean of the different ploidy levels (100% corresponds to a diploid population) in at least 10,000 cardiomyocyte nuclei of each analyzed heart sample. We also used published data of Adler on the ploidy distribution of children hearts to obtain the most comprehensive data collection (*12, 13*) (Fig. 3C).

An increase in the DNA content per nucleus during childhood leads to postnatal ^{14}C incorporation which is independent of cellular division. We used a computational approach to calculate polyploidisation independent delta ^{14}C values based on the atmospheric bomb curve and the polyploidisation time course in healthy individuals (Fig. 3D). In a first step, we calculated a regression curve that describes DNA content per nucleus with age f(a). We found that the sharp increase of DNA content around the age of six, can be best described by the following sigmoid curve with the parameters d_0=110.5, n=5.4, θ =7.0 and k=76.0 (R=0.955; SEE=10.149).

$$f(a) = d_0 H(a) + \frac{k}{1 + (\frac{a}{\theta})^{-n}}$$

No significant correlation after the age of ten between age and DNA content per nucleus is present during adulthood in healthy individuals (R=0.135, p=0.384) (Fig. 3C). In contrast to the stereotype time course of polyploidisation the individual adult DNA content per nucleus varies to a certain degree. Therefore we used the individual measured

DNA content per nucleus (DNA_i) to adjust ^{14}C values (C_{adj}) for polyploidisation (table S1). Value k dependent on adult DNA content is calculated as following and individual values of k are shown in the modeling supplement (supporting online text).

$$k = DNA_i - d_0$$

The change of DNA content can be described by the derivate of f: D(a) (see supporting online text for equation). For each subject of age a, at date t_{death} (born at calendar year t_{death}-a), the ^{14}C value was adjusted for polyploidisation ($C_{adj}(a)$).

$$C_{adj}(a) = \frac{\int_0^a K(t_{death} - a + s)\, D(s) ds}{\int_0^a D(s) ds}$$

The function K is the bomb curve (atmospheric ^{14}C levels). The denominator, the total DNA content at age a, is a normalization term.

The C_{adj} derived birthdate was determined for individuals born after the bomb spike (table S1). The age difference between the date of birth of the individual (DOB) and the C_{adj} derived birthdate was established. The obtained age difference was then subtracted from the average birth date of the cardiomyocytes population ($\Delta^{14}C$ derived birthdate), resulting in a ploidy independent average birth date of the cardiomyocyte population (Fig. 3D and table S1). For individuals born before the bomb-spike, ploidy independent ^{14}C values ($C_{independent}$) were calculated by subtracting the distance between the ^{14}C value at birth (C_{birth}) and the ploidy adjusted $\Delta^{14}C$ value (C_{adj}) from the measured $\Delta^{14}C$ value ($C_{measured}$) (Fig. 3D and table S1).

$$C_{independent} = C_{measured} - |C_{birth} - C_{adj}|$$

Human Ventricular Whole Cardiomyocyte Sorting

Human ventricular biopsy tissue was attained after consent to treatment and dissociated to single cell solution with Liberase Blendzyme 3 (0.1 mg/ml) (Roche Diagnostics), washed and spun down and resuspended in ice cold cardiomyocyte isolation buffer (130 mM NaCl; 5 mM KCl; 1.2 mM KH2PO4; 6 mM HEPES; 5 mM NaHCO3; 1 mM MgCl2; 5 mM Glucose). Cells were fixed with BD Cytofix/Cytoperm™ solution, permeabilised and incubated o/n at 4˚C with predetermined optimal concentrations of monoclonal antibodies to cardiac myosin heavy chain IgG1 ϰ (α- and β–MHC) (Abcam, ab15), α-smooth muscle actin IgG ϰ (α-SMA) (Abcam, ab32575) and CD31 IgG2a ϰ (Pecam-1) (eBioscience, 25-0311) in BD Perm / Wash™ Buffer in the dark on a shaker. Cells were washed and spun down twice and resuspended in secondary antibody cocktail containing predetermined optimal concentrations of donkey anti mouse Alexa Fluor® 488 (Molecular Probes™, Invitrogen A-21202) and donkey anti Rabbit Alexa Fluor® 647 (Molecular Probes™, Invitrogen A-31573), and appropriate isotype antibodies, in BD Perm / Wash™ buffer in the dark on a shaker at 4˚C for 3 hours. Cells were washed twice and resuspended in PBS and 5% FCS and then sorted on a BD FACSAria on low pressure with a 100μm nozzle.

Human Ventricular Cardiomyocyte Nuclei Isolation

Sorted cardiomyocytes were suspended in hypotonic buffer (0.01M Hepes and 1.5mM $MgCl_2$, pH 7.2) for 10 minutes on ice and then lysis buffer (3% glacial acetic acid and 5% ethylhexadecyldimethylammonium bromide in H_2O; Sigma) per 5ml of hyptonic buffer was added to washed cells, and tubes were shaken every minute for 10 minutes. The release of nuclei was examined by light microscopy. Nuclei were washed in nuclei wash

buffer (320 mM sucrose, 5 mM $MgCl_2$, 10 mM HEPES at pH 7.4) and spun down twice. Nuclei were then resupended in BD Perm / Wash™ buffer containing predetermined optimal concentrations of monoclonal mouse anti cTroponin I (Chemicon™, Millipore, MAB3152) and monoclonal cTroponin T (Neomarkers, Ab-1) Conjugated to Alexa Fluor® 647 with monoclonal antibody labeling kit (Molecular Probes™, Invitrogen A20186) for 3 hours in the dark on a shaker at 4˚C. Nuclei were washed in nuclei wash buffer and resupended in BD Perm / Wash™ buffer containing predetermined optimal concentration of donkey anti mouse Alexa Fluor® 488 (Molecular Probes™, Invitrogen A-21202) for 1.5 hours in the dark on a shaker at 4˚C. Appropriate isotype antibodies were also used. Nuclei were washed twice in nuclei wash buffer, resuspended in PBS passed through a 70μm filter and acquired on a BD FACSAria flowcytometer.

References and notes

1. G. L. de la Grandmaison, I. Clairand, M. Durigon, *Forensic Sci Int* **119**, 149 (Jun 15, 2001).
2. B. Brinkmann, *Int J Legal Med* **113**, 1 (1999).
3. K. L. Spalding, R. D. Bhardwaj, B. A. Buchholz, H. Druid, J. Frisen, *Cell* **122**, 133 (Jul 15, 2005).
4. R. P. Wersto *et al.*, *Cytometry* **46**, 296 (Oct 15, 2001).
5. S. Rozen, H. J. Skaletsky, in *Bioinformatics Methods and Protocols: Methods in Molecular Biology.,* K. S, M. S, Eds. (Humana Press, Totowa, NJ, 2000), pp. 365-386.
6. R. D. Bhardwaj *et al.*, *Proc Natl Acad Sci U S A* **103**, 12564 (Aug 15, 2006).
7. G. M. Santos, J. R. Southon, K. C. Druffel-Rodriguez, S. Griffin, M. Mazon, *Radiocarbon* **46**, 165 (2004).
8. J. S. Vogel, J. R. Southon, D. E. Nelson, *Nucl. Instrum. Methods Phys. Res. Sect. B* **29**, 50 (1987).

9. M. Stuiver, H. A. Polach, *Radiocarbon* **19**, 355 (1977).
10. T. A. Brown, J. R. Southon, *Nucl. Instrum. Methods Phys. Res. Sect. B* **123**, 208 (1997).
11. P. J. Reimer, T. A. Brown, R. W. Reimer, *Radiocarbon* **46**, (2004).
12. C. P. Adler, *Beitr Pathol* **158**, 173 (Jul, 1976).
13. C. P. Adler, in *The development and regenerative potential of cardiac muscle,* J. O. Oberpriller, J. C. Oberpriller, A. Mauro, Eds. (Harwood academic publishers, New York, 1991), pp. 227-252.

Supporting online text

The details of the mathematical models used to estimate the birth and death rates in cardiomyocytes and non-cardiomyocyte cells are presented in this text. It is organized as follows: 1. *Mathematical Model for Birth and Death*. 2. *Description of Eight Scenarios for Birth and Death*. 3. *Results*. 4. *Method for calculating ^{14}C content*. 5. *Alternative Model Formalism and Ploidy-Sorted ^{14}C data: Compartment Model*. 6. *Alternative Scenarios: Mature Cardiomyocyte Division and Heterogeneous Turnover*. Turnover models are discussed in section 2 and 3. Polyploidization is discussed in sections 3 and 5 and ploidy sorted data in section 5.

1. Mathematical Model for Birth and Death

The age-structured model for cell birth and death is specified by two functions: the cell death rate $\gamma(t,a)$ (units: per yr), and the birth rate of new cardiomyocytes from a stem cell pool $\beta(t)$ (units: cells per yr). It is useful to re-express the birth rate as a birth rate relative to the initial cardiomyocyte number N_0, $b = \beta/N_0$. Whenever we refer to the birth rate, it is always the relative birth rate. We assume that the number of cardiomyocytes is set to N_0 at birth. After that the cardiomyocyte number stays constant or is allowed to decrease according to published data.

The model may be formulated as a linear partial differential equation with an age-structure:

$$\frac{\partial n(t,a)}{\partial t} + \frac{\partial n(t,a)}{\partial a} = -\gamma(t,a)n(t,a) \qquad (1)$$

The function $n(t,a)$ is the density of cardiomyocyte of age a for a subject of age t relative to N_0 (unit of n: cell per year, units of a and t: year). The initial condition at $t = 0$ is $n(0,a) = N_0\ \delta_0(a)$, where δ is the Dirac delta function (i.e. all cells at $t = 0$ have age $a = 0$) and N_0 is the initial cardiomyocyte number. A boundary condition describes the birth of new cardiomyocytes from progenitor cells,

$n(t,0) = N_0$ (unit: cells per year). Equation 1, with the initial and boundary conditions, is related to the more general McKendrick-von Foerster equation used in population dynamics (1).

2. Description of Eight Scenarios for Birth and Death

The scenarios are ordered by increasing complexity, measured by the number of free parameters needed to specify the model.

In **Scenario A**, cell number is kept constant and cells turn over at a constant rate. There is only one parameter to estimate, allowing individual data points to be fitted. In **Scenario B**, the death rate and the birth rate can be different, and the cell number can change. In **Scenario C**, cell number is constant but the turnover rate is decreasing with the age of the individual (**C1** is linear-decreasing, **C2** is inversely proportional to age and **C3** is constant before a certain age and null after). In **Scenario D**, we made a cumulative damage hypothesis, for which cells have a higher replacement rate as they get older. In **Scenario E**, we made a cumulative survival hypothesis, for which cells have a lower replacement rate as they get older (**E1** is linear-decreasing and **E2** is inversely proportional to cell age). In Scenarios D and E, every dying cell is replaced so the cell number is constant. The birth rate $b(t)$ is determined by solving a Volterra equation of type II, or renewal equation (2):

$$b(t) = \gamma(t)\exp\left(-\int_0^t \gamma(s)\mathrm{d}s\right) + \int_0^t b(t-a)\gamma(a)\exp\left(-\int_0^a \gamma(s)ds\right)\mathrm{d}a$$

In **Scenario F**, there is cumulative damage and a constant birth rate. In **Scenario G**, there is constant death rate and a decreasing birth rate. In **Scenario H**, there is cumulative damage (or survival, depending on the parameter values) and decreasing birth rate. In scenarios F, G and H, cell number changes.

The goodness-of-fit is taken as the sum of squares of the errors (SSE) between the model prediction and the data $\sum_{i=1}^{n}(x_i - c_i)^2$, where x_i is the prediction and c_i is the $\Delta^{14}C$ level for subject i. All simulations were done with Matlab 7.

Table 1. Data and turnover for 12 subjects. The average turnover A was calculated in individual subjects using Scenario A. *Non-purity corrected. Parameter k is the individual gain in ploidy above the baseline d_0=110.5. Average continuous polyploidization values were computed using DNA content function f_2.

#	date of birth	age at death	$\Delta^{14}C$ purity corrected	k (ΔDNA content)	average turnover A (% per year)	average age of cardiomyocytes A (years)	avg turnover continuous ploidization (% per year)
ND60	1933.7	73.25	21.30*	79.5	0.28	66.3	0.10
ND67	1939.6	67.58	18.84	58.7	0.27	61.8	0.09
ND73	1944.6	62.67	3.65	72.2	0.15	59.8	0
ND61	1948.6	58.42	69.45	101.5	0.54	50.1	0.42
ND51	1955.9	50.83	194.60	57.4	0.79	41.8	0.40
ND56	1964.1	42.75	443.24	74.0	1.58	31.1	1.53
ND68	1967.4	39.83	403.08	52.7	1.36	30.8	1.14
ND50	1967.7	39.00	355.70*	83.1	1.65	28.8	1.63
ND69	1973.5	33.75	279.94	64.5	1.48	26.6	1.36
ND71	1983.5	23.75	178.40	74.5	0.90	21.4	0.93
ND54	1983.8	23.00	167.38	68.5	1.51	19.4	1.48
ND57	1987.2	19.67	141.20*	67.8	1.86	16.3	1.87

Table 2 Scenarios and global fitting results. The bomb curve was linearly interpolated. Parameters have appropriate units: γ is in year^{-1} and b in Initial Cell Number per year (ICN/year). Scenario C3 has two optimal fits (a and b). All simulations used tolerance < 1e-4 for numerical integration.

Scen.	Model	Nbr par.	Death rate	Birth rate	Fit	SSE (x10^4)	Comment
A	constant turnover	1	g = const	$b = g$	g = 0.010	2.77	good fit, but age-dependent turnover
B	constant death/birth	2	g = const	b = const	g = 0 b = 0.013	2.70	cell number increasing, lots of variability
C1	decreasing turnover, linear	2	$g(t) = \max\{g_0 - g_1 t, 0\}$	$b(t) = g(t)$	g_0 = 0.017 g_1 = 0.0003	2.64	poor fit
C2	decreasing turnover, inverse	2	$\gamma(t)=\gamma_0\gamma_1/(\gamma_1 + t)$	$b(t) = g(t)$	g_0 = 0.53 g_1 = 0.35	2.48	poor fit
C3a	decreasing turnover, step	2	$\gamma(t) = \gamma_0 H(\theta - t)$	$b(t) = \gamma(t)$	γ_0 = 0.0098 θ = 42.7	2.51	poor fit
C3b	decreasing turnover, step	2	$\gamma(t) = \gamma_0 H(\theta - t)$	$b(t) = \gamma(t)$	γ_0 = 0.45 θ = 6.1	3.29	poor fit
D	cumulative damage	2	$\gamma(a) = \gamma_0 + \gamma_1 a$	$b(t)$ solution of Volterra equation	γ_0 = 0.010 γ_1 = 0	2.77	no cumulative damage
E1	cumulative survival, linear	2	$\gamma(a) = \max\{\gamma_0 - \gamma_1 a, 0\}$	$b(t)$ solution of Volterra equation	γ_0 = 0.032 γ_1 = 0.0009	1.92	good fit
E2	cumulative survival, inverse	2	$\gamma(a)=\gamma_0\gamma_1/(\gamma_1 + a)$	$b(t)$ solution of Volterra equation	γ_0 = 0.123 γ_1 = 1.42	1.26	excellent fit
F	cumulative damage or survival, constant birth	3	$\gamma(a) = \max\{\gamma_0 - \gamma_1 a, 0\}$	$b = const$	γ_0 = 0.16 γ_1 = –0.0038 b = 0.0024	0.43	excellent fit but cell number too low
G	constant death, decreasing birth	3	$\gamma = const$	$b(t) = b_0 b_1/(b_1 + t)$	γ = 0.075 b_0 = 3.1 b_1 = 0.024	1.27	good fit, cell number too low
H	cumulative damage or survival, decreasing birth	4	$\gamma(a) = \max\{\gamma_0 + \gamma_1 a, 0\}$	$b(t) = b_0 b_1/(b_1 + t)$	γ_0 = 0.15 γ_1 = –0.003 b_0 = 0.86 b_1 = 0.098	0.25	Best fit but cell number too low

3. Results

Fitting individual subjects (Scenario A)

Scenario A has only one parameter, so it is possible to get an individual turnover estimate for each subject. We found an almost linear correlation between age and turnover rate for both pre- and post bomb patients (Main Text, Fig. 4A). The correlation is negative (R = – 0.84, Pearson's correlation p=0.001), indicating that older subjects have lower turnover rates. The turnover rates range from 0.0015 per year to 0.0186 per year (table 1). Therefore the constant turnover hypothesis (Scenario A) might not represent the turnover accurately, as as the turnover seems to be age-dependent.

Fitting all subjects (global nonlinear least-square parameter fitting, Scenario A to H)

To test the hypothesis that turnover is age-dependent, we compared eight scenarios (Scenario A to H, table 2). If the turnover is age-dependent, this may be because cells have a different turnover rate as they age (a-dependence), because the turnover depends on the age of the subject (t-dependence), or both. We fitted all eight scenarios to the 12 subjects, trying to find a common set of parameters that would be consistent with observed carbon levels. The description of the scenarios and the results of the fitting are in table 2. We first tried to find a constant turnover rate that would best predict the $\Delta^{14}C$ values observed in the subjects (Scenario A). The best value in the least-square sense is 0.0102 per year. The 95% confidence interval of the turnover CI = (0.006, 0.015) per year, does not include 0, it is therefore likely that the turnover is positive (p-value<0.05).

For several scenarios (A, B, C, D), there was a discrepancy between pre-bomb (born before 1955) and post-bomb (born after 1955) subjects. The models either overestimated the turnover rates in pre-bomb subject or under estimated the turnover in post-bomb subjects. This happened even for scenarios that included a turnover that decreased with the age of the individual. The only significant

improvement came from a-dependent scenarios (Scenario E, F and H), where a cell's probability to die changes as it gets older.

There is a small steady decline in cardiomyocyte number in aging hearts (3), indicating that new cardiomyocyte do not replace all dying cells. Ventricles can lose up to 0.5% of cardiomyocytes per year between ages of 20 and 70, leading to a 50% cell number reduction in aged ventricles. It is not clear whether the decreasing trend starts right after birth or there is a period in infancy and childhood when the cardiomyocyte number increases. A study in human suggests that there is no change in cell number in the first weeks after birth (4). Therefore, it is safe to assume that the cardiomyocyte number does not increase postnatally. In Scenarios B, F, G and H, we assumed that the cell number is not constant by allowing arbitrary death and birth rates. Scenario B (constant death and constant birth rates) predicted either a huge turnover (>5% per year, results not shown) or no cell death at all, leading to a significant increase in cardiomyocyte number. Both results are inconsistent with other scenarios and known cell number studies. Scenario F (a-dependent death rate and constant birth rate) performed better than fixed cell number scenarios, but predicts a sharp decrease in cell number (down to 5–10% of the initial cell number), inconsistent with the data from Olivetti et al. (3). The t-dependent Scenario G (constant death rate and decreasing birth rate) produced a good fit but a cell number too low. In Scenario H, we allowed an a-dependent death rate and a t-decreasing birth rate. This was the most sophisticated model we tested, and gave the best fit overall, but as in Scenario F, it predicts a low cell number that is inconsistent with cell number data (5–10% of initial cell number, similar to Scenario F).

Three main features came out of the simulations: (1) Scenario A captures well the average trend in turnover. (2) An a-dependent turnover is more consistent with the ^{14}C data than a t-dependent turnover. (3) Unless it is dramatic, a change in cell number does not improve the fitting to the data. In the simplest a-dependent models, Scenarios D and E, we assume that the death rate changes

monotonically as cells get older. Scenario D's best fit suggests that there is no cumulative damage effect, i.e., there is no increase in the death rate with cell aging ($\gamma_1 = 0$). Scenario E2, however, was consistent with the ^{14}C data, and predicted a significant decrease of turnover with age (Main Text, Fig. 4B).

Models with more parameters are expected to perform better, so a criterion that penalizes models with many parameters, such as the Akaike Information Criterion may be used for selecting the most parsimonious model. Akaike Information Criterion is $AIC = \log SSE + n_{par}$. It states that each additional parameter must reduce the SSE by a log. In log base 2, SSE must be halved for every additional parameter. According to *AIC*, the best models are Scenarios A, E, F, H (fig. 1, light gray bars). We conclude that a decreasing turnover is the scenario most compatible with both pre-bomb and post-bomb subjects. Because scenarios F and H predict a sharp decrease in cell number, results obtained with these scenarios should be interpreted with caution. Scenarios E are the most consistent with the data, and Scenario E2 has the lowest *AIC* (fig. 1). Since Scenario E2 reproduces the age-dependent decrease in turnover (Main Text, Fig. 4B), we verified that the parameter estimates for individual subjects were not age-dependent. To get individual estimates from Scenario E2, it is necessary to add one condition on the parameters, in addition to matching the $\Delta^{14}C$ levels. Either fixing one of the two parameters and fitting the other one, or constraining the parameters to be close to the globally fitted values gave similar results (not shown). Because fixing parameter γ_1 to a large value mimics Scenario A, we decided to minimize γ_1 in order to get the maximal range of parameter values admissible by Scenario E2. Individual estimates had a mean ± s.d. of $\gamma_0 = 0.13 \pm 0.04$ per year and $\gamma_1 = 1.0 \pm 0.4$ years, with no significant correlation with age (Pearson's correlation, p-value > 0.05). Parameter γ_1 is the age at which the replacement rate is half what it was at age 0. The globally fitted value for γ_1 is slightly larger than the minimal values for individual (1.4 years vs. 1.0 years).

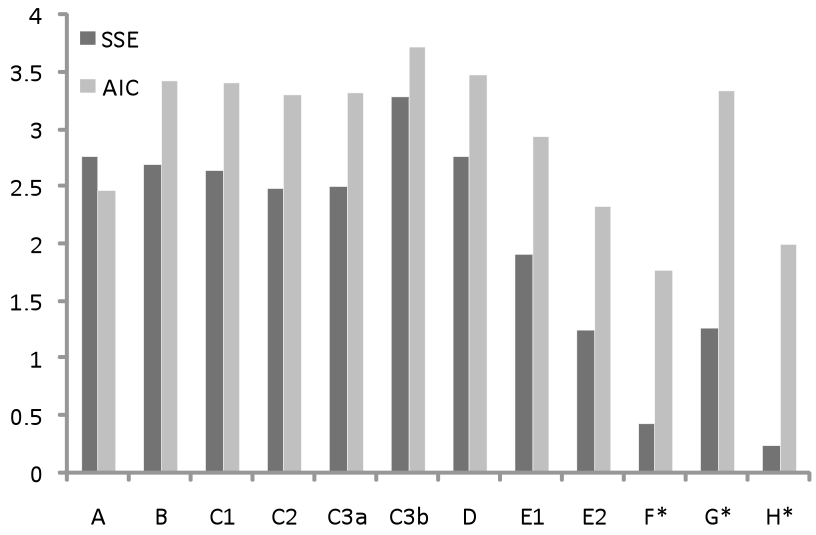

Figure 1. SSE ($x10^4$) and Akaike Information Criterion (AIC) for Scenarios A to H. *Predicts low cell number.

Effect of polyploidization in adult cardiomyocytes

It has been observed that hypertrophy in aging heart is associated with an increased ploidy, indicating that adult polyploidization can occur (5). To test whether adult ploidization affects the turnover estimates, we considered a DNA content function that is linear increasing after age 10 rather than constant ($f_2(a)$, see below). Because only cross-sectional data were available, it was not possible to determine the extent of ploidy increase in individuals. Instead, we used the range of the 95% interval confidence to find an upper bound on the possible increase in ploidy after age 10 (see Section 4 below). This leads to a 20 percentage points increase in DNA content after age 10 (from approximately 170% to 190%). The constant turnover scenario (Scenario A) predicts a global average turnover of 0.91% per year (SSE=$3.1x10^4$), slightly lower than the estimate from Scenario A. Individual average turnover rates show almost no changes in post-bomb subjects, while in pre-bomb subjects, turnover was reduced by half (table 1). Best decreasing turnover scenario (Scenario E2) predicts turnover parameters of γ_0=0.11 and γ_1=1.44 (SSE=$1.59x10^4$). This translates in a

turnover of 0.85% at age 25 and 0.36% at age 75, a reduction of 20% compared to no adult ploidization. These results indicate that with systematic polyploidization in adults, turnover rates would be up to 20% lower than estimated.

Adult polyploidization seems to affect post-bomb individuals only marginally, as mentioned above. We calculated the rate of ploidization that would be necessary to explain the ^{14}C if there were no turnover at all. The onset of ploidization was kept around 7 years, but adult ploidy was allowed to increase as much as necessary. In all post-bomb individuals the adult ploidy was unrealistically high (>300%), supporting that ^{14}C incorporation is due to turnover.

Nevertheless, since adult polyploidization mainly affected the oldest subjects, we tested whether it would be possible to explain ^{14}C integration by ploidization in these individuals. To characterize the variability of the ploidy levels, we used a sliding average with a window of width 9 (mean and STD are calculated for each 9 successive data points) on the ploidy data (fig. 2). In the adult range, the STD quickly stabilizes and there is no difference between a width of 9 and a width of 17. For width of 9, most data points lie within 1 STD (49 out of 62 or 79%, compared to 68% expected if data were normally distributed). Although there is a weak linear trend for an increase in ploidy with age, the sliding window shows that there is a decrease in ploidy in oldest subjects.

We calculated for the 5 pre-bomb individuals what the time course of ploidy should be if there were no turnover, on an individual basis. For one subject, there should be a decrease in ploidy, which has no biological meaning (this would be equivalent to adding negative ^{14}C). The other individual time courses are incompatible with the cross-sectional data. The 4 oldest subjects should all have begun adult life with a ploidy level lower than 1 STD from the mean ploidy. If ploidy levels are distributed normally in adults, the probability to observe ploidy levels lower than 1 STD from the mean in any subject is 0.159. This means that for the 4 pre-bomb subjects, the probability that they all had low ploidy at age 15 is $p = (0.159)^4 < 0.001$.

A linear increase might not best describe the time course of ploidy in adults. Adler & Friedburg (5) have shown that increase in ploidy is not associated with aging. DNA content (mg/g) was constant at all ages and heart weights, indicating that a change in heart weight accompanies polyploidization. We therefore considered a scenario where increase in ploidy is linked to pathology, i.e. occurs few years before death. We calculated the normal adult ploidy levels in the 5 pre-bomb patients if pathology-associated ploidization starts 10 years before death. The average DNA content for the 4 oldest subjects is 134% (2n=100%), well below the cross-sectional data average (data not shown). The fifth subject had a decreasing DNA content, which has no biological meaning, as in the previous case. We conclude that although ploidization in adults is possible and may contribute to ^{14}C integration, mitosis is necessary to explain the ^{14}C levels observed in pre-bomb subjects.

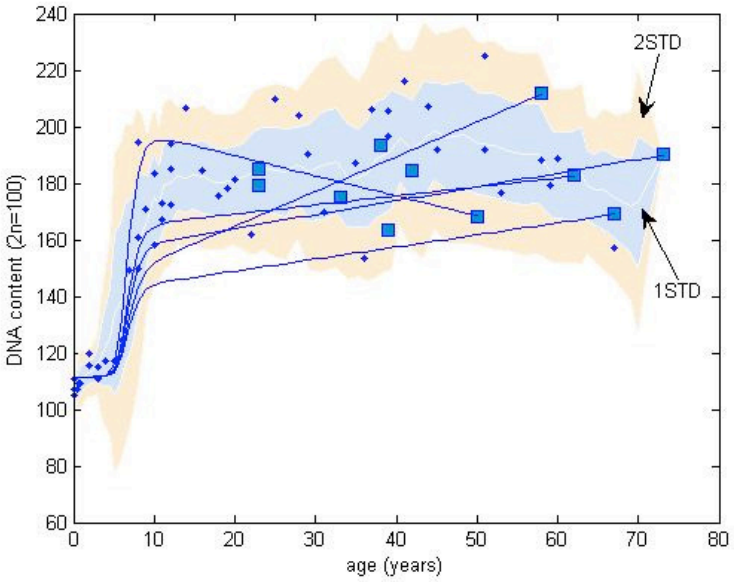

Figure 2. Ploidization-only scenario in pre-bomb subjects. DNA content (squares: subjects with ^{14}C data, dots: others, total n=62). The 1 STD (blue shading) interval based on a sliding window of with 9 includes most data points. None were outside 2 STD (pink shading). For the five pre-bomb patients, ^{14}C were fitted assuming ploidization only (solid lines). For the four ploidy time courses that were biologically relevant, all predicted unlikely ploidy levels in early adulthood.

Estimating the turnover rate in the non-cardiomyocyte fraction

The measured ^{14}C levels in unsorted cardiac cells allowed the purity correction in sorted cardiomyocytes. These values can also be used to estimate the turnover in the non-cardiomyocte fraction. We used the information about cardiomyocyte fraction in unsorted populations, cardiomyocyte DNA content (ploidy levels), unsorted cell ^{14}C levels, and calculated cardiomyocyte turnover parameters to estimate the^{14}C levels in the non-cardiomyocyte population. We then used the constant turnover scenario (Scenario A) to estimate turnover rates for 11 samples. We found a median turnover rate of the non-cardiomyocytes of 18% per year, corresponding to a mean age of 4.0 years (table 3). This estimate should be interpreted cautiously as it relies on indirect data and some estimated ^{14}C values are too low to correspond to any time point in the past. Nevertheless, these results suggest that, as expected, non-cardiomyocyte fraction turn over significantly faster than cardiomyocytes. There is no indication that the turnover is age-dependent.

Table 3. ^{14}C level and turnover estimates in non-cardiomyocytes. *Data not available. Instead, mean percentage of cardiomyocyte DNA and ploidy levels were used to estimate the ^{14}C content in non-cardiomyocytes.

case #	unsorted ^{14}C	myo DNA %	Estimated non cardiomyocyte ^{14}C	turnover (% per year)
ND67	50.03	52.43	84.41	16.87
ND73	32.26	49.98	60.85	41.83
ND61	51.62	66.36	16.45	0.29
ND59	31.70	56.56*	-122.48	0.00
ND51	115.00	47.57	42.76	0.46
ND56	275.70	55.77	64.42	37.64
ND68	227.12	58.51	-20.99	high
ND69	182.92	41.81	113.22	10.43
ND71	92.88	64.13	-60.02	high
ND54	144.30	72.51	83.42	17.54
ND74	96.53	56.56*	34.41	high

4. Method for calculating ^{14}C content

Polyploidization

To account for cell polyploidization, we introduce a function $D(a)$ that describes how much DNA is added in a cell of age a. The function $D(a)$ is the derivative of the DNA content function

$$f(a) = d_0 H(a) + \frac{k}{1 + \left(\frac{a}{\theta}\right)^{-n}},$$

where H is the Heaviside function, which takes the value 1 if $a \geq 0$ and 0 otherwise. The function f is introduced in section *^{14}C value correction for polyploidisation* of Supporting Materials and Methods. The parameters d_0, θ, and n are determined as described there, $d_0 = 110.5$, $\theta = 7.0$, and $n = 5.4$. The value k is the difference between adult DNA content and the baseline DNA content d_0 and is specific to each individual (table 1). This function is applied to the whole cardiomyocyte population and includes cells that turn over. To test the potential effect of polyploidization in adults, an alternative ploidy function with continuous ploidization in adults with a linear increase after age 10 was considered:

$$f_2(a) = d_0 H(a) + \frac{0.32a + 58}{1 + \left(\frac{a}{\theta}\right)^{-n}}$$

We used data from Fig. 3C in the main text. The linear part was chosen so that the ploidy spans the 95% percent confidence interval, from the lower limit at age ten to the upper limit at age 87 (the age of the oldest subject available). Other parameters are unchanged.

Carbon integration into cardiomyocyte DNA

The derivative of f is $D(a) = d_0 \delta(a) + \frac{kn\left(a/\theta\right)^{-n-1}}{\theta\left(1 + \left(a/\theta\right)^{-n}\right)^2}$.

The Dirac delta (δ) function is the derivative of the Heaviside function and represents the fact that DNA synthesized at the last cell division is synthesized during a very short interval compared to the time scale of interest (hours vs. years). For a given cell cohort of age a, at date t_{death} (born at calendar year $t_{death} - a$), the adjusted $\Delta^{14}C$ value is

$$C_{adj}(a) = \frac{\int_0^a K(t_{death} - a + s)D(s)\mathrm{d}s}{\int_0^a D(s)\mathrm{d}s}$$

The function $K(t)$ is the bomb curve (atmospheric $\Delta^{14}C$ levels) at calendar year t. The denominator, the total DNA content at age a, is a normalization term. The $\Delta^{14}C$ level from cardiomyocytes of a subject who died at t_{death} (calendar year) in a subject aged t year (born at calendar year $t_{death} - t$) is

$$C_{tot} = \frac{\int_0^t C_{adj}(a)n(t,a)\mathrm{d}a}{N(t)}.$$

The turnover estimates are relatively robust with respect to changes in parameter values used in function $D(a)$. Parameter θ, which controls the age of the peak in DNA synthesis, has the most important effect on turnover estimate. Parameter n control the width of the DNA synthesis period and d_0 and k control the minimal and maximal ploidy levels. To make sure that the results obtained with the age-structured models do not depend critically on the form of the ploidization function, we used a compartment model that includes explicitly cardiomyocyte ploidization.

5. Alternative Model Formalism and Ploidy-Sorted ^{14}C data: Compartment Model

The compartment model consists of the following equations

$$\frac{\partial n_2}{\partial t} + \frac{\partial n_2}{\partial a} = -(\gamma_2 + k_4 + k_{28})n_2\,,$$

$$\frac{\partial n_4}{\partial t} + \frac{\partial n_4}{\partial a} = -(\gamma_4 + k_8)n_4 + k_4 n_2\,,$$

$$\frac{\partial n_8}{\partial t} + \frac{\partial n_8}{\partial a} = -\gamma_8 n_8 + k_8 n_4 + k_{28} n_2$$

Initial conditions are

$$n_i(0,a) = n_i^0 \delta(a), \quad i = 2,4,8.$$

The cell densities $n_i(t,a)$ are the populations of ploidy i n. A boundary condition for n_2 is necessary to take into account birth of new cells,

$$n_2(t,0) = \beta.$$

Parameters γ_i are death rates and parameters k_i are ploidization rates. Keeping track of the ^{14}C content in each cell is a difficult task with the PDE system. An approach would be to introduce a new independent variable, c, which represent the DNA $\Delta^{14}C$ level. The cell density would become $n(t,a,c)$. This approach, however leads to an increase in the dimension of the system and raises numerical problems. To solve the system, we instead used a cellular automaton that has the advantage of tracking each cell individually instead of averaging large numbers of cells.

Model check

We first used the cellular automaton to check that the results obtained with age-structured models did not depend critically on the assumptions made about ploidization. In addition, we confirmed the

accuracy of the results obtained from the age-structured model against the cellular automaton (fig. 3). The ploidization parameters used are

$$k_4(a) = 0.9 \exp\left\{-(a-7)^2\right\},$$

$$k_8(a) = 0.05 \exp\left\{-(a-7)^2\right\}$$

(bell-shaped rates, units: per year). These parameters are age-dependent as it was impossible to get good ploidization curves from constant rate alone (ploidization was either too slow or the adult ploidy too large). The cellular automaton reproduces well the evolution of 2n, 4n and 8n ratios, and the total ploidy across ages (fig. 3A). The cellular automaton age-structured model (Scenarios A and E2) predict similar ^{14}C levels, indicating that the difference in modeling polyploidization is negligible (fig. 3B).

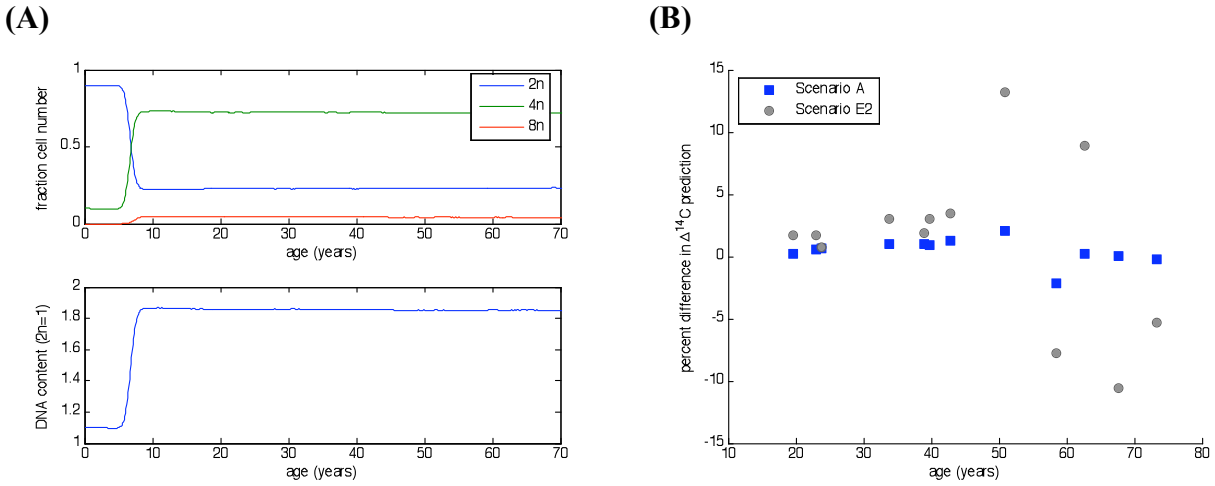

Figure 3. (A) Cellular automaton simulation, with optimal parameter fitted with Scenario A ($\gamma = 0.01$ per yr). (B) Comparison between the cellular automaton and the age-structured model (in percent difference relative to the cellular automaton simulations, for Scenario A, squares and E2, circles). Part of the difference comes from the variability in adult ploidy, which is taken into account in the age-structured model.

Ploidy-sorted data analysis

For three of the subjects, we had ^{14}C contents for 2n and 4n/8n cardiomyocytes (see table S2). The compartment model in best suited for ploidy-sorted data, because it takes into account the ploidy explicitly. Assuming constant turnover, a globally estimated 1.6% diploid cells are replaced every year in the three subjects (age ranges 23 to 33.7 years). This number is consistent with the values estimated for post-bomb subject, using all-ploidy ^{14}C values and taking into account polyploidization. Individual turnover estimates were also consistent with overall constant turnover values (ND69: 1.6% per year, ND71: 2.1% per year and ND54: 0.85% per year). Given the limited number of samples, it was not possible to detect trends or systematic differences in the turnover rates.

Polyploid cells (4n/8n) have a ^{14}C levels lower than 2n cells, as expected from the cross-sectional data showing that diploid cells undergo polyploidization in individuals between ages 7 and 10. According to these data, polyploid cells would be of the same age as diploid cells, but would appear younger due to ploidization. However, in addition to ploidization, differential turnover rates in cells of different ploidy can affect the measured ^{14}C values. We ran the cell automaton model, without turnover, to see what difference in apparent age between the 2n and the 4n/8n cells would be observed. Without turnover, diploid cells are as old as the individual. Tetraploid cells look slightly less than 3 years younger than the diploid cells (table 1). This is consistent with the phase of ploidization at age 7: 4n cells will have half the DNA aged 0 and half DNA aged 7. These values are also consistent with the bomb years associated to the sorted ^{14}C values, indicating that ploidization events can explain the difference measured. The “no turnover” ^{14}C values are all greater than what was measured, indicating that turnover occurs also in 4n/8n cells.

Table 4. No turnover ^{14}C values and bomb dates. "No turnover" predicts higher ^{14}C than measured.

subject	2n 14C / year	4n 14C / year	8n 14C / year
ND71	227 / 1983.3	196 / 1986	191 / 1986.6
ND69	428 / 1973.3	363 / 1975.9	350 / 1976.7
ND54	217 / 1984.1	187 / 1987	183 / 1987.5

Table 5. Turnover estimates of ploidy-sorted data. Birth and death rates are slightly different, so cell number is changing before settling to a new equilibrium (~10% change). *Indicates the maximal rate around age 7. Polyploidization rates are low otherwise. **For simplicity, 8n cells come from newborn cells only.

subject	death rate (per year)	birth rate (IC per year)	ploidization rates*	calculated ^{14}C
ND71	0.018	0.0059	0.8	185
	0.0096	0.0032	0**	181
	0.003	0.001	-	118
ND71 total	-	0.0101	-	178
ND69	0.023	0.0076	0.45	318
	0.015	0.005	0**	283
	0.05	0.0017	-	140
ND69 total	-	0.0142	-	279
ND54	0.016	0.0053	0.5	196
	0.016	0.0053	0**	173
	0.03	0.0033	-	111
ND54 total	-	0.0139	-	169

We then looked at what would be the turnover of 4n/8n cells if polyploidization events were entirely associated to birth of new cell (all DNA synthesized at the same time). A turnover rate of 2.6% percent per year was estimated. This value provides an upper bound for the turnover rate with the ^{14}C values measured, but it is not consistent with the time course of ploidy. A middle ground must be found somewhere that is consistent with ploidy time courses and the ^{14}C levels.

Including newborn cells of high ploidy in the cell automaton involved a few changes. In the original model, cardiomyocyte regeneration rate involved only the diploid compartment. The birth rate was β cells/year. Now β must be split between the three ploidy compartment: $\beta = \beta_2+\beta_4+\beta_8$. There are now 8 parameters: β_2, β_4, β_8, γ_2, γ_4, γ_8, k_2, k_8. The last parameters control the polyploidization rates of existing cells. Results of individual fits are shown in table 5. Comparison of the turnover rates using

different methods shows that estimates are quite robust (table 6). Estimates for subject ND69 are consistent for all models tested. In subject ND71 and ND54, estimates for 2n cells only are quite different. This probably can be explained by the inverse relationship between 14C levels in diploid and all cells.

Table 6. Summary turnover rates estimated under various ploidization conditions (in % per year). All ploidy: individual estimates from Scenario A. 2n only: individual estimates from Scenario A using calculated 2n ^{14}C values sorted cardiomyocytes. Ploidy-sorted: individual estimates using the cell automaton model. Continuous ploidization: individual estimates using continuous adult ploidization.

	all ploidy	2n only	ploidy-sorted	continuous ploidization
ND69	1.52	1.59	1.42	1.40
ND71	0.98	2.08	1.01	1.01
ND54	1.59	0.85	1.39	1.55

6. Alternative Scenarios: Mature Cardiomyocyte Division and Heterogeneous Turnover

Mature cardiomyocyte division

The model takes into account polyploidization of mature cardiomyocytes, but not the division, for example of a mononucleated cell that would become binucleated (synthesing DNA) and then divide. What the birth rate measures is the formation of new cardiomyocytes from cardiac stem/progenitor cells. If a mature cardiomyocyte divided symmetrically after duplicating DNA, the daughter cells would look younger than the mother cell but still older than a newborn cell (half the DNA would be old, unless DNA is perfectly segregated). However, their pooled DNA would have the same ^{14}C content distribution as an old cell and a newborn cell, making the mature cardiomyocyte division process undistinguishable from the birth of a new cardiomyocyte from a precursor. Although there would be no difference in the turnover rate (one cell added has the same effect on the ^{14}C measurement), the cell age distribution would differ. This could have some influence on the mathematical formulation of models that are age-dependent, as the age of the cell would not be

necessarily determined by the age of its DNA. The consequences of these small differences on the average age estimates have not yet been fully explored.

Heterogeneous turnover

Apart from having all cardiomyocytes turning over with the same probability, there is the possibility that a subset of cardiomyocytes never turn over while other subsets turn over frequently. A correct description of turnover must lie between these two opposite scenarios. To see whether heterogeneous turnover can explain the observed ^{14}C levels, we used an alternative model where the cardiomyocytes are divided into two populations, 1 and 2, where Population 1 does not turn over and Population 2 turns over rapidly. The total population is kept constant: $N_1(t) + N_2(t) = N_0$. This leads to a modified expression for the total $\Delta^{14}C$ levels in samples

$$C_2 = \frac{N_1(t)}{N_0} C_{adj}(t) + \frac{N_2(t)}{N_0} C_{adj}(0).$$

Here, we made the assumption that cells in Population 2 are virtually new born, i.e. the turnover is infinite. Any lower turnover will make this alternative model closer to the default one. If a difference is to be seen, it is with this extreme example. The first term of C_2 gives the $\Delta^{14}C$ levels of cells present at birth that do not turnover, while the second term gives the $\Delta^{14}C$ levels of newborn cells (at the collection date). The proportion of cell in Population 2 and Population 1 are given by the fractions $p = N_2/N_0$ and $(1 - p)$ respectively. Because the total population is constant, only one parameter—the fraction p of renewing cells—needs to be estimated. A global least-square fit gave $p = 0.33$. Thus 33% percent of the cardiomyocytes would have to be contemporary while the other 67% present from birth to yield the same measured average $\Delta^{14}C$. The best fit, when a slower turnover in the renewing subset is allowed, gives a turnover of 9% per year, with a renewing fraction that increases to 38% only (SSE=0.47×10^4). Thus, a change of few percents of the fast turnover

fraction implies large changes in the turnover rate. This makes it rather difficult to estimate the turnover rates but gives us a lower bound of 33% for the fraction turning over.

This subset would have to be a specific region of the myocardium, because the random nature of cell death already implies that a fraction of cells evenly distributed in the myocardium will never turn over (Scenario E2 predicts that half of initial cells are still present in a 75 year old subject). Based on the assumption that the subset is associated to a particular region of the heart, one would expect the percentage of renewing cardiomyocytes to be relatively uniform among individuals, composing in average at least $p = 1/3$ of the cardiomyocytes.

When the samples are fitted individually, either using a fixed fraction p or a fixed turnover rate, there are unrealistic values ($p > 1$ or infinite turnover rates). In addition, pre-bomb sample can be fitted by two different values because of the shape of the bomb curve, leading to difficulties in the interpretation of the results. When both the fraction p and the turnover rate are allowed to change, many solutions are possible. Some of them might be realistic, but without additional information their relevance cannot be evaluated. Although a global fit of all the samples gives good results, individual samples speak against a well-defined subset of cardiomyocytes that would turn over, while the remaining cardiomyocytes are static. These results must be interpreted in the context where the size or the content of the subset does not change in time.

References

1. Perthame, B, *Transport Equations in Biology*, (2007) Birkhäuser Basel

2. Linz, P, *Analytical and Numerical Methods for Volterra Equations*, (1985), SIAM Philadelphia

3. Olivetti G, Melissari M, Capasso JM, Anversa P. (1991) Cardiomyopathy of the aging human heart. Cardiomyocyte loss and reactive cellular hypertrophy. *Circ Res.* **68**:1560-1568

4. Austin A, Fagan DG, Mayhew TM. (1995) A stereological method for estimating the total number of ventricular cardiomyocyte nuclei in fetal and postnatal hearts. *J Anat.* **187** (Pt 3), 641-647

5. Adler CP, Friedburg H. (1986) Myocardial DNA content, ploidy level and cell number in geriatric hearts: post-mortem examinations of human myocardium in old age. *J Mol Cell Cardiol.* **18**:39-53.

A

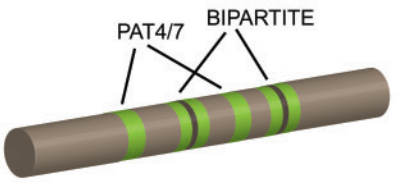

cardiac Troponin T
TNNT2

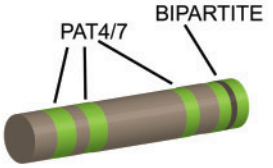

cardiac Troponin I
TNNI3

B

C

Protein	PSORT II NLS (Bipartite)	PSORT II %Nuclear	NucPred Score	Specificity
TNNT2 H. sapiens	4 (2)	73.9	0.87	0.84
Tnnt2 M. musculus	4 (2)	78.3	0.86	0.84
TNNT2 G. gallus	4 (3)	82.6	0.93	0.88
upheld (f) D. melanogaster	5 (4)	82.6	0.94	0.88
TNT-2 C. elegans	2 (1)	69.6	0.81	0.84
GATA-4 H. sapiens	1	82.6	0.64	0.71
MYL2 H. sapiens	1	8.7	0.11	0.45

Protein	PSORT II NLS (Bipartite)	PSORT II %Nuclear	NucPred Score	Specificity
TNNI3 H. sapiens	4 (1)	73.9	0.75	0.81
TNNI3 M. musculus	4 (1)	73.9	0.73	0.81
TNNI3 G. gallus	3 (2)	87.0	0.76	0.81
wings up D. melanogaster	3 (3)	78.3	0.71	0.81
Ce TNI-3 C. elegans	3 (3)	87.0	0.65	0.71
GATA-4 H. sapiens	1	82.6	0.64	0.71
MYL2 H. sapiens	1	8.7	0.11	0.45

Figure S1

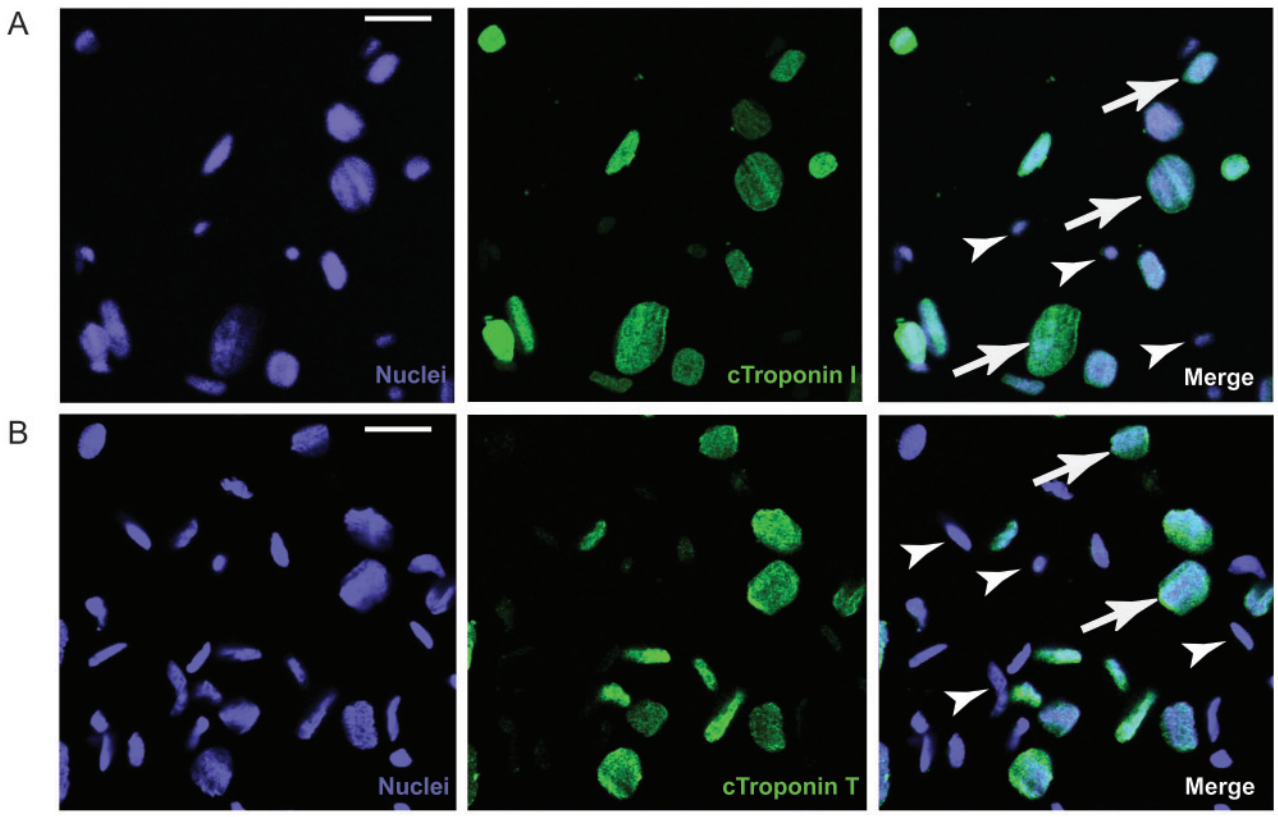
A
Nuclei
cTroponin I
Merge
B
Nuclei
cTroponin T
Merge

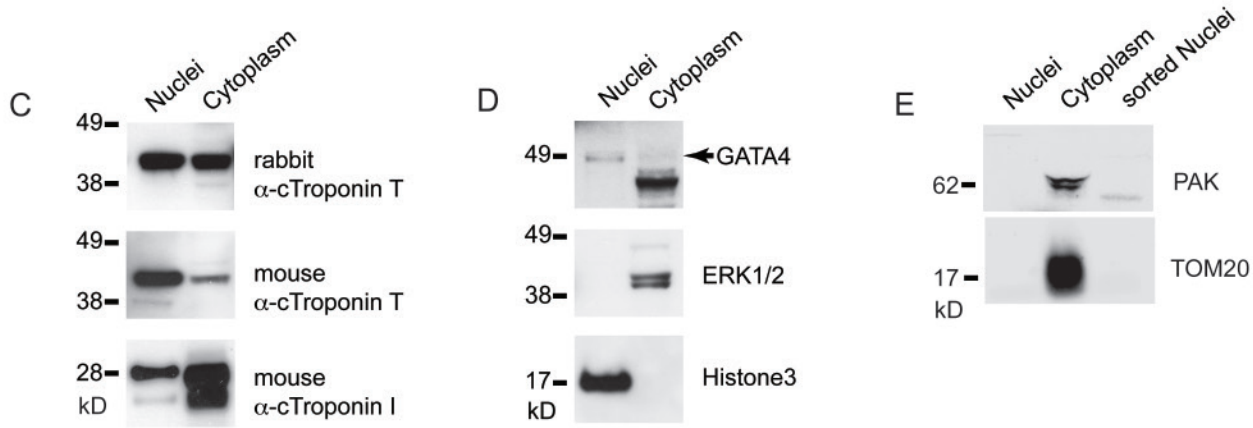
C
Nuclei
Cytoplasm
49
38
rabbit
α-cTroponin T
49
38
mouse
α-cTroponin T
28
kD
mouse
α-cTroponin I
D
Nuclei
Cytoplasm
49
GATA4
49
38
ERK1/2
17
kD
Histone3
E
Nuclei
Cytoplasm
sorted Nuclei
62
PAK
17
kD
TOM20

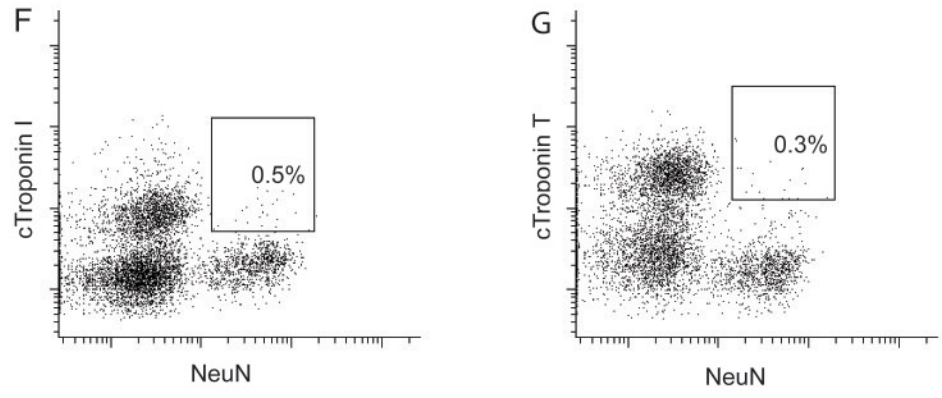
F
cTroponin I
0.5%
NeuN
G
cTroponin T
0.3%
NeuN

Figure S2

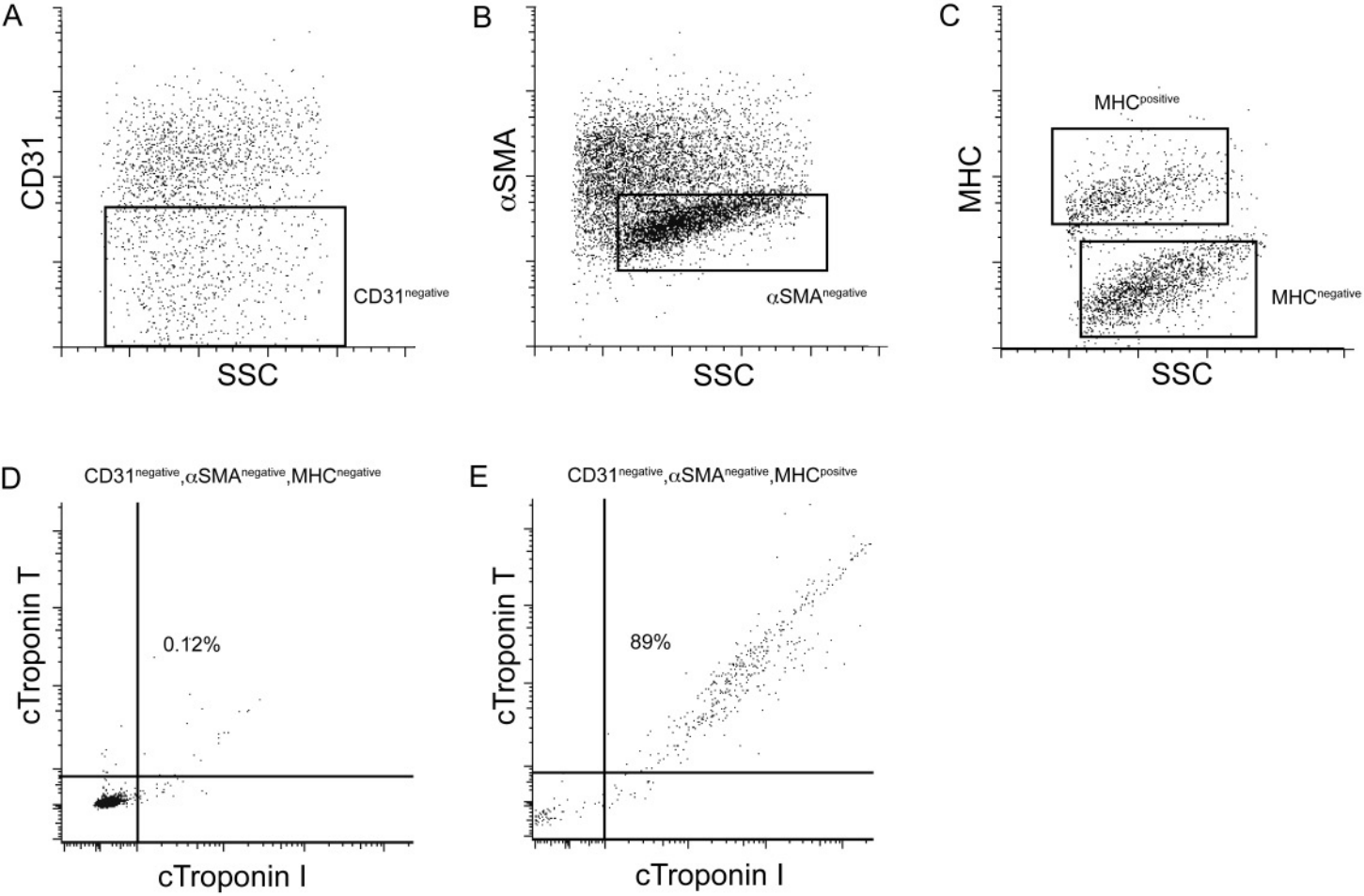
A
CD31
CD31negative
SSC
B
αSMA
αSMAnegative
SSC
C
MHCpositive
MHC
MHCnegative
SSC
D
CD31negative,αSMAnegative,MHCnegative
0.12%
cTroponin T
cTroponin I
E
CD31negative,αSMAnegative,MHCpositve
89%
cTroponin T
cTroponin I

Figure S3

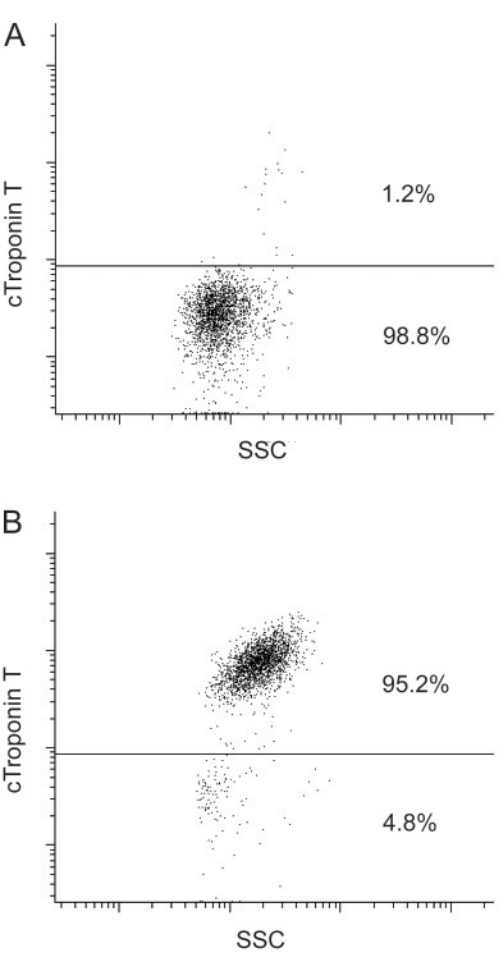

Figure S4

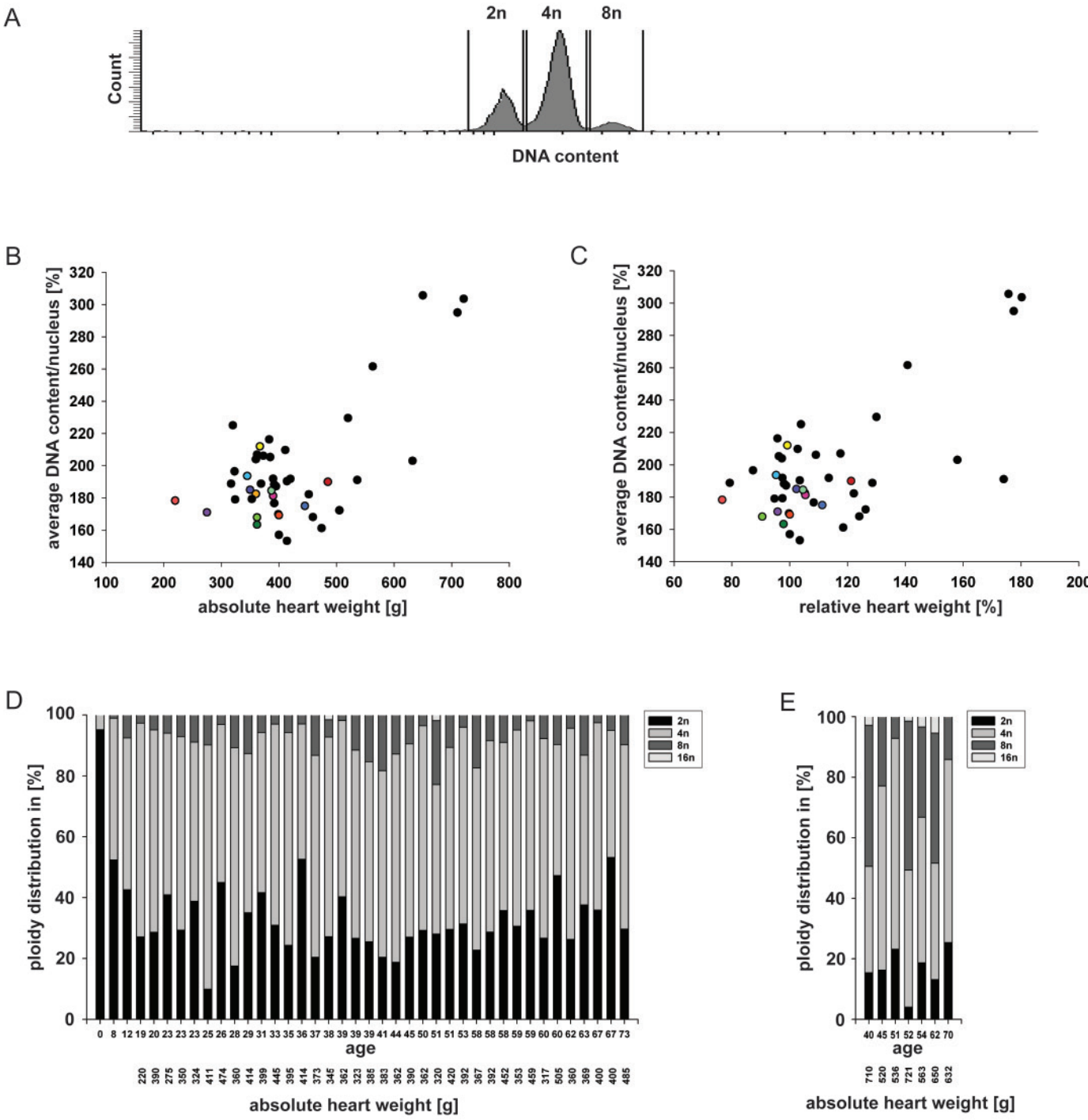
A
2n
4n
8n
Count
DNA content
B
average DNA content/nucleus [%]
absolute heart weight [g]
C
average DNA content/nucleus [%]
relative heart weight [%]
D
ploidy distribution in [%]
2n
4n
8n
16n
age
absolute heart weight [g]
E
ploidy distribution in [%]
2n
4n
8n
16n
age
absolute heart weight [g]

Figure S5

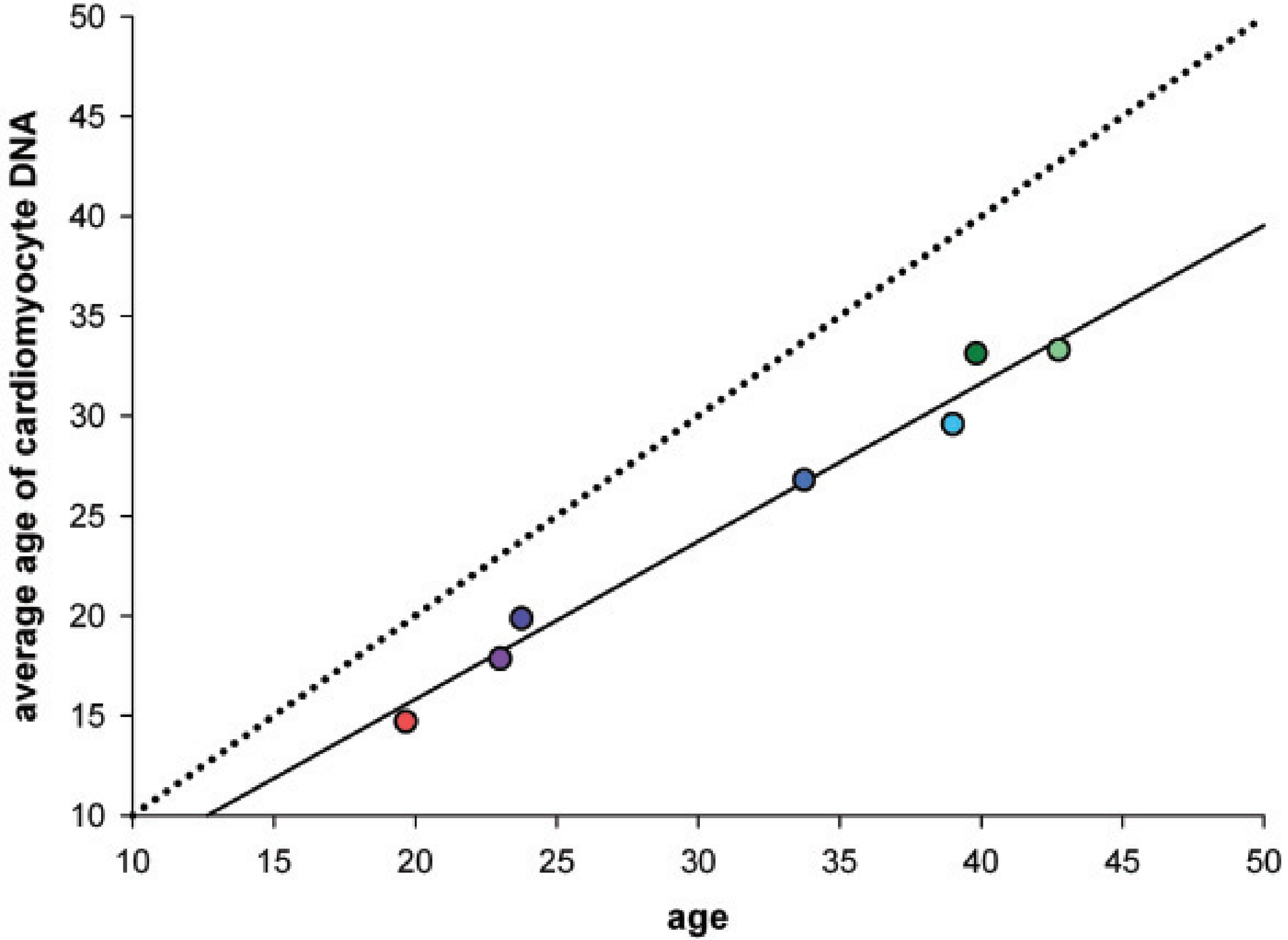
average age of cardiomyocyte DNA
50
45
40
35
30
25
20
15
10
10
15
20
25
30
35
40
45
50
age

Figure S6

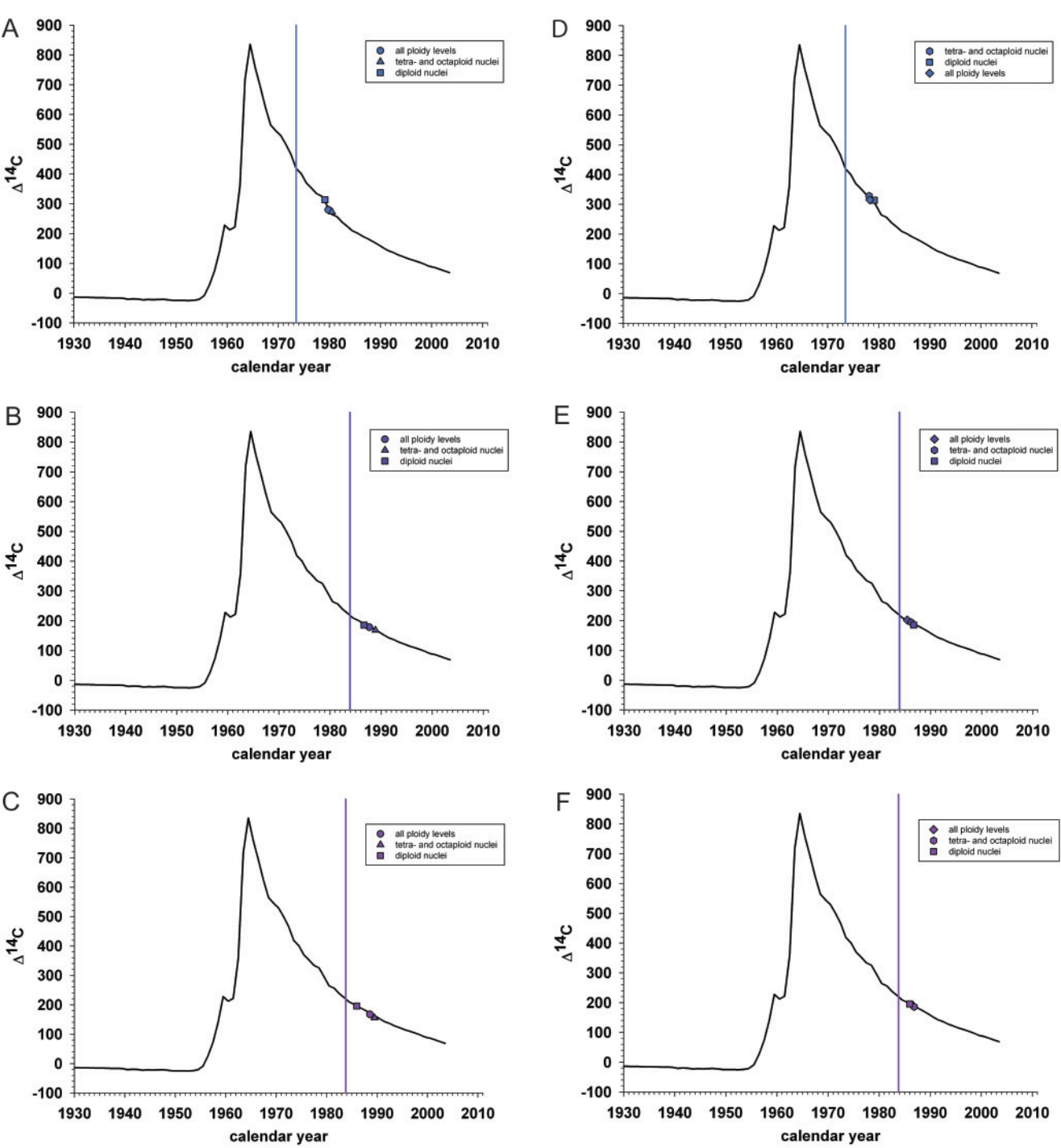
A
B
C
D
E
F
Δ14C
calendar year
all ploidy levels
tetra- and octaploid nuclei
diploid nuclei

Figure S7

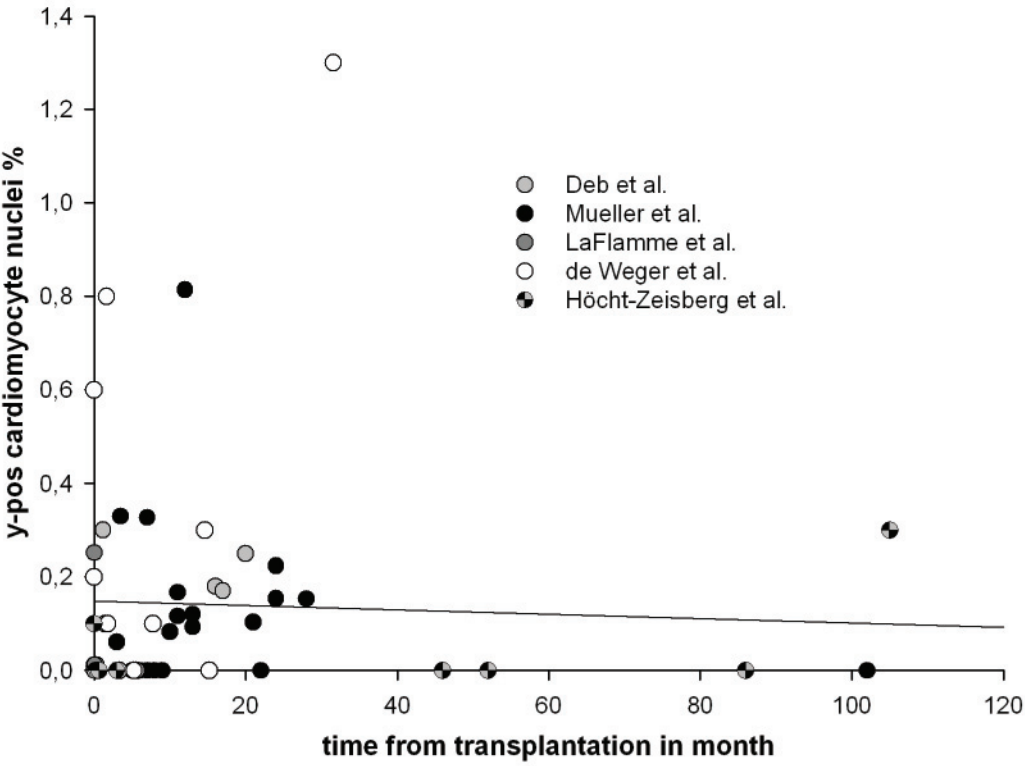
1,4
1,2
1,0
0,8
0,6
0,4
0,2
0,0
y-pos cardiomyocyte nuclei %
Deb et al.
Mueller et al.
LaFlamme et al.
de Weger et al.
Höcht-Zeisberg et al.
0
20
40
60
80
100
120
time from transplantation in month

Figure S8

case #	Flow cytometry sorted population	sex	DOB	DOD	age	DOM	$\Delta^{14}C$	±	^{14}C derived birthdate	± years
ND60	TropI	male	Sep-33	Dec.06	73	2007	21.30	12.00	*	*
ND67	TropT	male	Aug-39	Mar.07	67	2007	20.80	9.25	*	*
ND73	TropT	male	Aug-44	Apr-07	62	2007	7.70	7.55	*	*
ND61	TropI	male	Aug-48	Jan-07	58	2007	68.60	9.42	*	*
ND51	TropT	male	Nov-55	Sep-06	50	2007	186.71	9.95	*	*
ND56	TropI	male	Feb-64	Nov-06	42	2006	430.10	10.60	1973.40	0.77
ND68	TropT	male	May-67	Mar.07	39	2007	377.83	14.81	1975.15	1.80
ND50	TropI	female	Sep-67	Sep-06	38	2006	355.70	32.20	1976.42	3.24
ND69	TropT	male	Jun-73	Mar 07	33	2007	271.14	20.79	1980.89	2.58
ND71	TropT	male	Jun-83	Mar 07	23	2007	165.60	6.17	1988.34	1.75
ND54	TropI	female	Oct-83	Oct 06	23	2006	163.60	8.40	1988.58	2.00
ND57	TropI	female	Mar-87	Nov-06	19	2006	141.20	10.20	1991.30	2.74
ND67	unsorted	male	Aug-39	Mar.07	67	2007	50.03	3.68	1956.23	0.73
ND73	unsorted	male	Aug-44	Apr-07	62	2007	32.26	4.57	1956.13	0.63
ND61	unsorted	male	Aug-48	Jan-07	58	2007	51.62	3.95	1956.23	0.73
ND59	unsorted	male	Sep-53	Dec 06	53	2006	31.70	16.00	1954.21	3.11
ND51	unsorted	male	Nov-55		50	2006	115.00	8.90	1957.63	0.34
ND56	unsorted	male	Feb-64	Nov-06	42	2006	275.70	13.40	1980.42	1.52
ND68	unsorted	male	May-67	Mar 07	39	2007	227.12	8.68	1982.70	1.44
ND69	unsorted	male	Jun-73	Mar 07	33	2007	182.92	4.85	1986.71	1.39
ND71	unsorted	male	Jun-83	Mar 07	23	2007	92.88	7.04	1998.53	2.89
ND54	unsorted	female	Oct-83	Oct.06	23	2006	144.30	6.20	1990.92	1.78
ND74	unsorted	male	Feb-87	Apr-07	20	2007	96.53	4.95	1998.01	2.40

case #	DNA content/nucleus (%) 2n=100 4n=200 8n=400	cardiomyocyte fraction in %	DNA content/nucleus weighted Flow cytometry purity in %	$\Delta^{14}C$ Flow cytometry purity corrected	birthdate Flow cytometry purity corrected	$\Delta^{14}C_{adj}$*	$^{14}C_{adj}$ derived* birthdate	polyploidisation independent $\Delta^{14}C$	polyploidisation independent birthdate	number of ^{14}C dated nuclei in millions
ND60	189.97	34.80	96.45	21.30	*	-16.31	*	19.73	*	27.70
ND67	169.20	39.45	97.00	18.84	*	-18.08	*	17.72	*	89.90
ND73	182.74	35.35	93.00	3.65	*	-17.77	*	-0.24	*	45.80
ND61	212.00	48.20	98.40	69.45	*	9.96	*	36.96	*	35.00
ND51	167.94	35.08	94.80	194.60	*	169.26	*	28.73	*	57.00
ND56	184.50	40.60	96.53	443.24	1972.67	672.05	1966.64	*	1970.13	31.00
ND68	163.21	46.35	94.04	403.08	1973.87	557.09	1968.99	*	1972.28	68.20
ND50	193.64	45.28	97.22	355.70	1976.42	516.68	1970.37	*	1973.75	33.10
ND69	175.03	29.10	96.50	279.94	1980.20	365.81	1975.68	*	1978.03	57.10
ND71	185.01	49.15	94.63	178.40	1987.14	195.43	1985.62	*	1985.03	56.50
ND54	179.02	59.57	95.50	167.38	1988.17	192.73	1985.90	*	1986.07	56.00
ND57	178.31	58.20	98.86	141.20	1991.30	161.36	1988.53	*	1989.98	37.30
ND67	169.20									>100
ND73	182.74									>100
ND61	212.00									>100
ND59										>100
ND51	167.94									>100
ND56	184.50									>100
ND68	163.21									>100
ND69	175.03									>100
ND71	185.01									>100
ND54	179.02									>100
ND74	181.20									>100

* see supplement for detailed description: 14C value correction for polyploidisation

Table S1

case #	age	cause of death	absolute heart weight at autopsy in [g]	Body Mass Index BMI	Estimated normal heart weight* according to BMI [mean+1SD]	relative heart weight [%]	Heart Enlargement*	Hypertrophy	Fibrosis	Coronar Sclerosis	Hypertension	Diabetes mellitus	Hypercholesteremia	Smoking	Cardiovascular Medication	Other Diseases	Other Medication
ND50	38	suicide (intoxication)	345	32	362+77	95.30	no	slight	no	no	no	no	no	no	no	no	antidepressants, tranquilizers
ND51	50	multiple trauma	362	27	400+69	90.50	no	no	no	no	no	no	not determined	no	no	no	no
ND54	23	suicide (hanging)	275	18	287+74	95.82	no	no	no	no	no	no	no	no	no	no	antidepressants, tranquilizers
ND56	42	suicide (intoxication)	387	23	370+75	104.59	no	slight	no	no	yes	no	no	no	no	psoriasis	hypnotics, tranquilizers, NSAID, opiates
ND57	19	multiple trauma	220	23	287+74	76.66	no	no	no	no	no	no	not determined	no	no	no	antidepressants
ND59	53	suicide (intoxication)	300	19	348+58	86.21	no	no	no	slight	no	no	no	yes	no	COPD	benzodiazepines, opiates
ND60	73	acute myocardial infarction	485	28	400+69	121.25	yes	slight	yes	moderate-severe	no	no	slight	no	nitrates	ischemic stroke 1988, old heart infarction	NSAID
ND61	58	multiple trauma	367	22	370+75	99.19	no	slight	slight	slight	no	no	no	no	no	no	no
ND67	67	acute myocardial infarction	400	25	400+69	100.00	no	yes	no	moderate	no	no	slight	no	no	no	no
ND68	39	suicide (hanging)	362	23	370+75	97.84	no	no	no	no	no	no	no	yes	no	depression	hypnotics, antidepressants
ND69	33	suicide (intoxication)	445	34	400+69	111.25	no	no	no	no	no	no	no	yes	no	no	analgetics, anabolic steroids, benzodiazepines
ND71	23	multiple trauma	350	21	348+58	100.57	no	no	no	no	no	no	no	yes	no	depression	antidepressants, NSAID
ND73	62	suicide (hanging)	360	17	348+58	103.45	no	no	no	slight	no	no	no	no	no	ALS	benzodiazepines, opiates
ND74	20	suicide (suffocation + intoxication)	390	23	370+75	105.41	no	slight	no	no	no	no	no	no	no	no	analgetics

*de la Grandmaison et al. 2001

Table S2

case #	Flow cytometry sorted population	sex	DOB	DOD	age	DOM	$\Delta^{14}C$	±	^{14}C derived birthdate	± years
ND69	TropT	male	Jun-73	Mar 07	33	2007	271.14	20.79	1980.89	2.58
ND69	TropT diploid nuclei (2n)*	male	Jun-73	Mar 07	33		301,98*		1978.82	
ND69	TropT higher ploidies (4n8n)	male	Jun-73	Mar 07	33	2007	264.10	9.70	1980.81	1.22
ND71	TropT	male	Jun-83	Mar 07	23	2007	165.60	6.17	1988.34	1.75
ND71	TropT diploid nuclei (2n)	male	Jun-83	Mar 07	23	2007	174.10	17.30	1987.26	1.97
ND71	TropT diploid nuclei (2n)*	male	Jun-83	Mar 07	23		173.03*		1987.59	
ND71	TropT higher ploidies (4n8n)	male	Jun-83	Mar 07	23	2007	164.20	4.30	1988.72	0.70
ND54	TropI	female	Oct-83	Oct 06	23	2006	163.60	8.40	1988.58	2.00
ND54	TropI diploid nuclei (2n)*	female	Oct-83	Oct 06	23		188,71*		1986.25	
ND54	TropI higher ploidies (4n8n)	female	Oct-83	Oct 06	23	2006	155.70	6.50	1990.49	0.72

case #	Flow cytometry sorted population	DNA content/nucleus weighted Flow cytometry purity in %	$\Delta^{14}C$ Flow cytometry purity corrected	birthdate Flow cytometry purity corrected	$\Delta^{14}C_{adj}$*	$^{14}C_{adj}$ derived* birthdate	polyploidisation independent birthdate	number of ^{14}C dated nuclei in millions
ND69	TropT	96.50	279.94	1980.20	368.55	1975.43	1978.27	57.10
ND69	TropT diploid nuclei (2n)*		313.22	1978.22				
ND69	TropT higher ploidies (4n8n)	93.98	271.46	1980.48	358.40	1975.85	1978.13	56.53
ND71	TropT	94.63	178.40	1987.14	197.07	1985.19	1985.45	56.50
ND71	TropT diploid nuclei (2n)	82.77	185.02	1986.27				25.50
ND71	TropT higher ploidies (4n8n)	96.60	168.14	1987.98	194.30	1985.28	1986.20	146.00
ND54	TropI	95.50	167.38	1988.17	194.21	1985.41	1986.56	56.00
ND54	TropI diploid nuclei (2n)*		195.61*	1985.60				
ND54	TropI higher ploidies (4n8n)	96.47	155.45	1989.15	186.10	1986.12	1986.86	38.50

* ^{14}C values calculated

Table S3

Legends to Supporting Figures and Tables

Figure S1. Nuclear localization signals (NLS) within cTroponin T (TNNT2) and cTroponin I (TNNI3).

Since non-cardiomyocytes are very adherent to and are often in very close proximity to cardiomyocytes within the myocardium, a strategy based on cell sorting may not allow for the desired purity as it may be difficult to exclude cell doublets. Since a substantial proportion of cardiomyocytes are binucleate, it is not possible to avoid doublets by excluding cells with more than two nuclei. By choosing to sort for cardiomyocyte nuclei as opposed to whole cells, we could better control purification and still obtain the desired DNA.

(A) We took a bioinformatic approach to search for predicted nuclear localization signals within cytoplasmic cardiomyocyte markers. We found that cTroponin T (TNNT2) (left panel) and cTroponin I (TNNI3) (right panel) both contain four putative nuclear localization signals. **(B)** NucPred ClustalW alignment between species shows the relative basic residue content and distribution (positive=more likely nuclear). Species display a similar NLS organisation near the N-termini of the protein. **(C)** Table showing specifity for nuclear localization of cTroponin T and I for different species. Nuclear GATA4 (NP_002043.2) and cytosolic cardiac myosin light chain were used as positive and negative controls, respectively. Specificity represents the binned fraction of proteins predicted to be nuclear that have been experimentally confirmed (greater is more reliable).

Figure S2. cTroponin T and cTroponin I are both present in cardiomyocyte nuclei.

(A, B) To verify the nuclear localization, a nuclear isolate from left ventricular tissue was incubated with DAPI (which labels DNA and reveals all nuclei) and antibodies against cTroponin I **(A)** or cTroponin T **(B)**. cTroponin I and T-immunoreactivity was present in a subset of nuclei that were larger in size than the unlabeled nuclei. Arrows point to cTroponin I and cTroponin T-immunoreactive nuclei and arrowheads to negative nuclei. Scale bars are 20µm. **(C)** We next performed Western blot analyses to further characterize the cTroponin I and cTroponin T-immunoreactive epitopes in the nuclei. Analysis of heart tissue separated into a cytoplasmic and a nuclear fraction by centrifugation revealed the presence of cTroponin I (approx. 28 kDa and 25kDa) and cTroponin T (approx. 40 kDa) in the cytoplasm as well as in the nuclei (left panel). The two different cTroponin I bands have been suggested to represent different phosporylation states (*1, 2*). Interestingly, one kinase known to phosphorylate cTroponin I is the nuclear protein TNNI3K, in line with the presence of the putatively phosphorylated form in the nucleus (*3*). **(D, E)** ERK1/2 and PAK detection only in the cytoplasm, and GATA4 as well as Histone 3 detection only in the nuclei, confirmed the purity of both cellular fractions. **(E)** TOM20, a import receptor protein localized in the outer mitochondrial membrane, was highly enriched only in the cytoplasmic fraction, demonstrating little mitochondrial contamination both in the flow cytometry sorted nuclear fraction (third lane) and in the nuclear fraction purified by sucrose cushion (first lane). **(F, G)** To address whether transfer of free cTroponin I or T to nuclei may occur,

resulting in false positive labeling, we mixed brain and heart tissue and analyzed whether neuronal nuclei were labeled with antibodies against cTroponin I **(F)** and cTroponin T **(G)**. Since this protein is not expressed in the brain, labeling of neuronal nuclei would indicate the transfer of this protein to the nuclei. We did not find labeling of neuronal nuclei (NeuN-positive) above background levels (0.3-0.5%), arguing against transfer of cTroponin I or cTroponin T to noncardiomyocyte nuclei during the isolation strategy.

Figure S3. cTroponin T and cTroponin I are both present in adult cardiomyocyte nuclei in human heart tissue biopsies.

Human left ventricular cardiomyocytes were isolated from human bioptic heart tissue by means of flow cytometry. Cardiomyocytes were defined as $CD31^{negative}$ (**A**), α-$SMA^{negative}$ (**B**) and $MHC^{positive}$ (**C**) and sorted accordingly. Nuclei from the $CD31^{negative}$, α-$SMA^{negative}$, $MHC^{positive}$ population (cardiomyocytes) and $CD31^{negative}$, α-$SMA^{negative}$, $MHC^{negative}$ population (negative control) were extracted subsequentially and reanalyzed by flow cytometry. cTroponin I and cTroponin T were not detected above background level (0.12%) in non-cardiomyocyte nuclei (**D**) whereas 89% of all cardiomyocyte nuclei were positive for both cTroponins (**E**). Abbreviations: SMA=smooth muscle actin; MHC=cardiac myosin heavy chain.

Figure S4. Reanalysis of flow cytometric sorted myocardial nuclei.

(A) Representative flowcytometric plot depicting cTroponin T-negative fraction with a contamination of 1.2% cTroponin T-positve nuclei. **(B)** Re-analysis of flow cytometric sorted cTroponin T-positive fraction with a contamination of 4.8% of cTroponin T-

negative nuclei.

Figure S5. Flow cytometric analysis of DNA content in human cardiomyocyte nuclei. **(A)** Representative flowcytometric plot showing different DNA levels of sorted human cardiomyocyte nuclei. Nuclei were incubated with Hoechst33342 (5μg/ml) before analysis. Average DNA content per cardiomyocyte nucleus [%] in left ventricles (wall and apex) is presented against absolute heart weight **(B)** and relative heart weight **(C)**. No correlation exists between relative heart weights up to 130% (*4*) and average DNA content per nucleus (R=0.08; p=0.621). All ^{14}C dated heart samples, depicted as colored dots, have relative heart weights <130% (see table S2). A positive correlation between heart weight and average DNA content per nucleus does exist only from absolute heart weights >500g and relative heart weights >130%. **(D)** Percentage distribution of ploidy levels (DNA content) of human hearts having relative weights <130% according to BMI (*4*) or **(E)** relative heart weights >130% depicted sequentially with the age of the subjects. Different grayscales indicate different ploidy levels. 2n=diploid DNA. Absolute heart weights [g] were determined as described in the Materials and Methods and in (*4*).

Figure S6. Continuous DNA synthesis in cardiomyocytes.

The age of the individual is plotted against the average age of cardiomyocyte DNA from individuals born after the bomb spike. The dotted line represents the no cell turnover scenario, where the average age of cardiomyocytes equals the age of the individual. The black line shows the best fitting for all data points (R=0.991; p<0.001). The difference

between the birth date of the person and the date corresponding to the ^{14}C level in cardiomyocyte DNA increased with the age of the individual.

Figure S7. Cardiomyocyte DNA of all ploidy levels is younger than the individual.

(A, B, C) The ^{14}C levels in cardiomyocyte DNA of all measured ploidy levels correspond to time points after the birth of the individuals. Diploid cardiomyocyte DNA is older than tetra- and octaploid DNA in all depicted subjects. **(D, E, F)** ^{14}C levels in cardiomyocyte DNA corrected for polyploidization (see supporting online text) indicate similar ^{14}C integration in diploid and polyploid cardiomyocyte DNA. The vertical bar indicates year of birth, with the correspondingly colored data point indicating the ^{14}C values for diploid (squares), tetra- and octaploid nuclei (triangles and polygons for ploidy independent values) and for all cardiomyocyte ploidy levels (dots and diamonds for ploidy independent values).

Figure S8. Y-chromosome chimerism in human heart after gender-mismatch heart or bone marrow transplantation.

Cell fusion is a potential source of non-cardiomyocyte DNA which could bias our interpretation of cell turnover. After gender-mismatched heart or bone marrow transplantation, several studies could show chimeric y-chromosome positive cardiomyocytes in the female heart. This phenomenon has been explained by cell fusion events or transdifferentiation of host/donor cells into differentiated cardiomyocytes (*5-7*). Most studies analyzing cardiomyocytes found a low level of chimerism (0% to 1.3%, median: 0.037%) with no correlation with time after transplantation (R=0.046, p=0.74)

(*5, 8-11*) nor with the age of the patient (R=0.232; p=0.086). Bayes-Genis et al. showed that the degree of chimerism in the human heart decreased by in average 38% when investigating the same individuals at 4 and 12 months after transplantation, arguing for chimerism being a temporally limited acute rather than a continuous occurring physiological phenomenon (*12*). Other studies even failed to find any evidence for cardiomyocyte chimerism (*13-15*). Two reports, however, found a much higher number of chimeric cardiomyocytes (6.4-18%) (*16, 17*) which is most likely an overestimation due to the infiltration of host-derived leukocytes into the heart and different detection techniques (*5, 11, 18*). The described low frequency of cardiomyocyte positive y-chromosomes and the transient nature of chimerism in the human heart could not explain the DNA turnover that we report here (supporting online text). Therefore neither transdifferentiation of non-cardiac stem cells into cardiomyocytes nor potential cell fusion events seems to be responsible for the observed cardiomyocyte turnover.

Table S1. Data set for all ^{14}C-dated subjects.

Table showing all data from 14 individuals whose myocardial DNA was carbon dated. DOB = date of birth, DOD = date of death, DOM = date of measurement. For a complete explanation of the terms '$\Delta^{14}C$' and 'Flow cytometry purity corrected $\Delta^{14}C$', 'C_{adj}' and 'polyploidisation independent $\Delta^{14}C$ values', refer to Material&Methods. All $\Delta^{14}C$ derived birthdates were determined by applying pMC values to the software provided on the freely accessible CALIbomb web site (http://calib.qub.ac.uk/CALIBomb/frameset.html). We used the Levin dataset and a smoothing and resolution value of one year.

Table S2. Pathological assessment and medical history of all ^{14}C-dated cases.

Comprehensive pathological assessment and medical history of all cases are presented. Heart enlargement was assessed by using tables for normal heart weights according to BMI (*4*). Hearts were considered to be enlarged if the absolute heart weight was higher than mean+ 1SD heart weight according to BMI.

Table S3. ^{14}C levels in DNA in cardiomyocyte nuclei separated based on DNA content

Table showing data from 3 subjects whose myocardial ploidy levels (DNA content) were separately carbon dated. DOB = date of birth, DOD = date of death, DOM = date of measurement. The ^{14}C values for the diploid ND54 and ND69 data points ($C_{diploid}$) were calculated based on the ^{14}C levels for higher ploidies ($C_{tetra+octaploid}$) and for all ploidy levels ($C_{allploidies}$), respectively. To validate our calculation for the ^{14}C concentration of diploid nuclei, we compared the measured and calculated diploid ^{14}C concentration of case number ND71. The calculated ^{14}C value differed <0.7% from the actual ^{14}C concentration.

$$C_{all\ ploidies} \times (ratio[\%]_{diploid} + DNAfactor \times ratio[\%]_{tetra+octaploid}) =$$

$$C_{diploid} \times ratio[\%]_{diploid} + C_{tetra-octaploid} \times DNAfactor \times ratio[\%]_{tetra+octaploid}$$

DNAfactor refers to the average DNA content per nucleus, $ratio[\%]_x$ refers to the ratio in percentage of the respective ploidy compartment (e.g. diploid). For a complete explanation of the terms 'Δ^{14}C' and 'Flow cytometry purity corrected Δ^{14}C', 'C_{adj}' and 'polyploidisation independent Δ^{14}C values', see Materials and Methods. All Δ^{14}C derived

birthdates were determined by applying pMC values to the software provided on the freely accessible CALIbomb web site (http://calib.qub.ac.uk/CALIBomb/frameset.html). We used the Levin dataset and a smoothing and resolution value of one year.

References and notes

1. A. Schmidtmann, K. Lohmann, K. Jaquet, *FEBS Lett* **513**, 289 (Feb 27, 2002).
2. D. G. Ward *et al.*, *Biochemistry* **43**, 5772 (May 18, 2004).
3. Y. Zhao *et al.*, *J Mol Med* **81**, 297 (May, 2003).
4. G. L. de la Grandmaison, I. Clairand, M. Durigon, *Forensic Sci Int* **119**, 149 (Jun 15, 2001).
5. M. A. Laflamme, D. Myerson, J. E. Saffitz, C. E. Murry, *Circ Res* **90**, 634 (Apr 5, 2002).
6. S. Zhang *et al.*, *Circulation* **110**, 3803 (Dec 21, 2004).
7. E. Minami, M. A. Laflamme, J. E. Saffitz, C. E. Murry, *Circulation* **112**, 2951 (Nov 8, 2005).
8. A. Deb *et al.*, *Circulation* **107**, 1247 (Mar 11, 2003).
9. E. Hocht-Zeisberg *et al.*, *Eur Heart J* **25**, 749 (May, 2004).
10. P. Muller *et al.*, *Circulation* **106**, 31 (Jul 2, 2002).
11. R. A. de Weger *et al.*, *Bone Marrow Transplant* **41**, 563 (Mar, 2008).
12. A. Bayes-Genis *et al.*, *Cardiovasc Res* **56**, 404 (Dec, 2002).
13. I. Bittmann *et al.*, *Am J Clin Pathol* **115**, 525 (Apr, 2001).
14. R. H. Hruban *et al.*, *Am J Pathol* **142**, 975 (Apr, 1993).
15. R. Glaser, M. M. Lu, N. Narula, J. A. Epstein, *Circulation* **106**, 17 (Jul 2, 2002).
16. F. Quaini *et al.*, *N Engl J Med* **346**, 5 (Jan 3, 2002).
17. J. Thiele *et al.*, *Pathologe* **23**, 405 (Nov, 2002).
18. D. A. Taylor, R. Hruban, E. R. Rodriguez, P. J. Goldschmidt-Clermont, *Circulation* **106**, 2 (Jul 2, 2002).